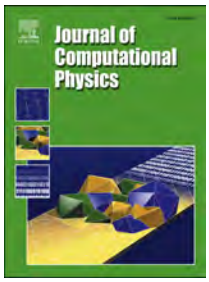

The use of proper orthogonal decomposition (POD) meshless RBF-FD technique to simulate the shallow water equations

Mehdi Dehghan*, Mostafa Abbaszadeh

[a]Department of Applied Mathematics, Faculty of Mathematics and Computer Sciences,
Amirkabir University of Technology, No. 424, Hafez Ave.,15914, Tehran, Iran

September 6, 2017

Abstract

The main aim of this paper is to develop a fast and efficient local meshless method for solving shallow water equations in one- and two-dimensional cases. The mentioned equation has been classified in category of advection equations. The solutions of advection equations have some shock, thus, especial numerical methods should be employed for example discontinuous Galerkin and finite volume methods. Here, based on the proper orthogonal decomposition approach we want to construct a fast meshless method. To this end, we consider shallow water models and obtain a suitable time-discrete scheme based on the predictor-corrector technique. Then by applying the proper orthogonal decomposition technique a new set of basis functions can be built for the solution space in which the size of new solution space is less than the original problem. Thus, by employing the new bases the CPU time will be reduced. Some examples have been studied to show the efficiency of the present numerical technique.

Keywords: Meshless method, proper orthogonal decomposition (POD) procedure, shallow water equations, radial basis functions(RBF), local collocation method, finite difference (FD) method, local moving Kriging interpolation.

Mathematics Subject Classification: 26A33, 49M30, 33C45

1 Introduction

A wide variety of physical and natural phenomena such as sound, heat, electrostatics, electrodynamics, fluid flow or elasticity have been described using partial differential equations (PDEs). We refer the interested reader to [104] for various applications of partial differential equations in sciences and engineering and also for some approaches in obtaining their solutions.

*Corresponding author. *E-mail addresses:* mdehghan@aut.ac.ir , mdehghan.aut@gmail.com (M. Dehghan), m.abbaszadeh@aut.ac.ir (M. Abbaszadeh).

The shallow water (SW) equations can be considered as a simplification of the Navier-Stokes equations [102]. In the shallow water models, the horizontal wave length is much larger than the depth of the fluid [102]. For this reason, some special numerical methods such as discontinuous Galerkin, finite volume and adaptive moving mesh methods can be used for solving the advection problems.

1.1 A brief review on SWs equations

In the current paper, we consider three boundary value problems in water science:

1. **The 1D and 2D shallow water equations without friction term:**
   Trahan and Dawson [101] investigated a second-order, local time stepping procedure within a Runge-Kutta discontinuous Galerkin (RKDG) framework to solve the shallow water equations. The dam-break problems in one- and two-dimensional shallow water equations are attractive problems in numerical analysis and many investigations have been done on these problems. The public solution for the dam-break problem has been developed by Cozzolino and his co-workers [31].

   Benkhaldoun and his co-workers [2] developed a new stabilized meshless method based on the radial basis functions for the numerical solution of convection-dominated flow problems. This class of problems includes viscous Burgers equations and incompressible Navier–Stokes equations at high Reynolds numbers. A new finite volume method has been proposed in [3] based on the predictor stage and a corrector stage for the numerical solution of shallow water equations for either flat or non-flat topography. The main aim of [4] is to propose slope limiters in meshless radial basis functions for solving nonlinear equations of conservation laws with flux function that depends on discontinuous coefficients as the method is based on the local collocation formulation. Authors of [1] presented the similarity solution to the Riemann problem of the one dimensional shallow water equations (SWE) with a bottom step discontinuity. Using the class of fractional-step procedures, a simple and accurate projection finite volume method is developed in [5] for solving shallow water equations in two-space dimensions. A new class of finite volume method is presented in [6] for solving shallow water flows in porous media on unstructured triangular grids in which the method consists of two stages which can be interpreted as a predictor-corrector procedure.

   Navas-Montilla and Murillo [82] proposed an arbitrary accurate derivatives Riemann problem (ADER) type finite volume numerical scheme as an extension of a first-order solver with source terms. Li and his co-workers [67] proposed a numerical procedure for shallow water equations with a source term as the equations admit steady state solutions in which the non-zero flux gradient is exactly balanced by the source term. Xing [106] developed well-balanced discontinuous Galerkin approaches for the shallow water system. Sun and his co-authors [95] applied the meshless local RBF differential quadrature (LRBFDQ) technique to simulate the shallow water equations (SWE).

   A well-balanced, spatially arbitrary with high order accurate discontinuous Galerkin scheme is proposed by Tavelli and Dumbser [100]. Canestrelli and his co-workers [19] studied on finite volume method for the 2D shallow water equations. Dumbser and Casulli [39] developed a spatially arbitrary high-order, semi-implicit spectral discontinuous Galerkin (DG) scheme for

the shallow water equations.

The main aim of the current paper is to develop a combined RBF-FD approach to solve some shallow water equations. The RBF-FD approach is constructed by combining radial basis functions concept and finite difference method. In the finite difference technique, the corresponding weights can be obtained by using local polynomial approximations. Also, radial basis functions can be chosen instead as basis functions translates of radially symmetric functions. Thus, combination of radial basis functions with finite difference approach leads to radial basis function-generated FD formulas. Furthermore, all approximations again local, but nodes can now be placed freely.

One local meshless method is smoothed particle hydrodynamics (SPH) that is presented in [48, 76]. The SPH technique is a computational method used for simulating the dynamics of continuum media, such as solid mechanics and fluid flows. The SPH method is a mesh-free Lagrangian method where the coordinates move with the fluid, and the resolution of the method can easily be adjusted with respect to variables such as the density. The SPH method is based on the dividing the fluid into a set of discrete elements that they are well-known as "particles". These particles have a spatial distance over which their properties are "smoothed" by a kernel function. This means that the physical quantity of any particle can be obtained by summing the relevant properties of all the particles which lie within the range of the kernel. Also, the SPH method is employed for the shallow water equation. The interested readers can find more information on SPH method in [118]

Wei and et. al. [119] applied the SPH method to investigate the impact of a tsunami bore on simplified bridge piers in this study. This work was motivated by observations of bridge damage during several recent tsunami events. The main aim of [120, 121] is apply the numerical model of GPUSPH, an implementation of the weakly compressible Smoothed Particle Hydrodynamics method on graphics processing units, to investigate tsunami forces on bridge superstructures and tsunami mitigation on bridges by using a service road bridge and an offshore breakwater. Authors of [122] investigated vorticity generation by short-crested wave breaking by using the mesh-free Smoothed Particle Hydrodynamics model.

Katta and his co-workers [63] developed a central-upwind finite volume (CUFV) scheme for solving shallow water model on a nonorthogonal equiangular cubed-sphere grid. High-order spatial discretization based on weighted essentially non-oscillatory (WENO) scheme is considered in [63].

Cotter and Thuburn [29] described discretisations of the shallow water equations on the sphere using the framework of finite element exterior calculus. They presented [29] two formulations as follows:

- "primal" formulation in which the finite element spaces are defined on a single mesh
- "primal-dual" formulation in which finite element spaces on a dual mesh are used.

Felcman and Kadrnka [43] applied the moving mesh method to the shallow water equations. An upwind weighted essentially non-oscillatory scheme for the solution of the shallow water equations on generalized curvilinear coordinate systems is proposed by Gallerano and his co-workers [49]. Bistrian and Navon [13] proposed a framework for dynamic mode decomposition

(DMD) of 2D flows, when numerical or experimental data snapshots are captured with large time steps.

Also, for solving shallow water models that are introduced in the current subsection, we can mention that Xing and Shu [107] developed a high order finite difference WENO scheme, Xing et. al [108] developed simple positivity-preserving limiter, valid under suitable CFL condition based on the discontinuous Galerkin method, Xing and Shu [109] proposed a high-order accurate finite volume weighted essentially non-oscillatory (WENO) scheme, and Noelle and et. al [83] presented a new high–order accurate, exactly well–balanced finite volume scheme.

2. **The 1D and 2D shallow water equations with friction term:**
The studied hydrostatic upwind scheme in [9] is extended for considering 2D simulations performed over unstructured meshes. Authors of [10] investigated the late-time asymptotic behavior of solutions to nonlinear hyperbolic systems of conservation laws containing stiff relaxation terms. They proposed [10] a new finite volume discretization which, in late-time asymptotics, allows us to recover a discrete version of the same effective asymptotic system. The main aim of [11] is to present a new scheme to compute the friction source terms in the shallow-water model. The main aim of [12] is to analyze some ambiguities coming from a class of sediment transport models in which the models under consideration are governed by the coupling between the shallow-water and the Exner equations. Authors of [38] considered a finite volume numerical approximation of weak solutions of the shallow water equations with varying topography, on unstructured meshes.

3. **The 2D shallow water model with sediment concentration**:
This model is presented in [50] and [77, 125]. Also, authors of [77] proposed a new proper orthogonal decomposition finite difference method with error estimate.

1.2 A brief review on RBF and RBF-FD techniques

Meshless methods are constructed based on scattered nodes in the problem domain [75, 17]. Radial basis functions collocation method is known as Kansa's method [61, 62]. A famous RBF is MQ function that is introduced by Hardy [54].

The local RBF-FD collocation method is a new technique to solve bad-posed problems. The RBF-FD idea is developed in [34, 91, 92, 93, 94, 98, 99, 123]. There exist several research works on RBF-FD technique for example Flyer et. al [45] established the computational efficiency and accuracy of the RBF-FD method, Fornberg and Lehto [46] developed a filter approach for RBF-FD, Fornberg and his co-workers [47] developed the RBF-GA algorithm to work effectively for up to a few hundred node points in 2-D, Bollig et. al [14] proposed some parallelization strategies for the RBF-FD method, Javed and his co-authors [59] studied a novel concept of adaptive shape parameter for RBF-FD technique, Gonzalez-Rodriguez et. al [51] developed an algorithm to overcome the inherent ill-condition in the computation of RBF-FD weights, Sarra [87] proposed a local RBFs collocation method for system of advection-reaction-diffusion equations with Neumann boundary condition on irregular domains and Islam and his co-workers [57, 58] presented an improved localized RBFs collocation method (LRBFCM) for hyperbolic PDEs.

Chan and his co-workers [21] developed a new upwind technique based on the local radial basis function differential quadrature (LRBF-DQ) method to solve the convection-dominated flow

problems. Interpolation techniques based on the local radial basis function differential quadrature (LRBF-DQ) method are proposed in [22] to interpolate the field values with arbitrarily given scattered data. The main aim of [95] is to apply the meshless local radial-basis-function differential quadrature (LRBFDQ) method to solve the shallow water equations (SWE). Authors of [124] developed the local radial basis function (RBF) scheme to simulate 2D and 3D heat transfer and flow dynamics of generalized Newtonian fluids (GNF).

The shape parameter in the radial basis functions has an important role in stability and convergence of numerical algorithms based on the radial basis functions. Also, several studies have been done to select an optimal shape parameter [86]. Especially, Bayona and his co-workers [15, 16] proposed an optimal shape parameter for the local RBF-FD technique. Authors of [15] developed an efficient algorithm to compute the optimal value of the shape parameter that minimizes the approximation error. A novel technique to compute the solution of PDEs with the multiquadric based local RBF finite difference method (RBF-FD) using an optimal variable shape parameter c_j at each node of the computational domain is presented in [16] . Also, we refer the interested reader to [28, 90] for useful investigations on meshless method of radial basis functions and some related issues.

The shape functions of moving Kriging interpolation are similar to the moving least squares approximation. These shape functions rather have properties of the shape functions of moving least squares approximation. The shape functions of moving Kriging have the δ-Kronecker property. The interested researchers can find more information for the moving Kriging interpolation technique in [18, 27, 33, 72, 52, 53, 67, 88, 89, 128, 129, 127]. The shallow water equation is a conservation law equation thus a global RBFs collocation method with global support is not suitable for solving this model. In other hand, as is said in [57] to overcome the problems of ill-conditioning and shape parameter sensitivity of the global RBFs collocation method, the local radial basis functions collocation method has been used.

1.3 Proper orthogonal decomposition (POD) approach

Proper orthogonal decomposition (POD) method is a principal component analysis, the Karhunen-Loève transform, or singular value decomposition (SVD), POD (Berkooz et al. [7] 1993; Everson and Sirovich [40] 1995; Kerschen et al. [64] 2005) are powerful statistical tool to transform a large set of correlated variables into a small number of variables that are uncorrelated. As a result, a compressed representation of the original data is obtained. The representation is optimal in the sense that the mean-squared reconstruction error is minimized.

The POD technique is a powerful approach to reduce the used CPU time which is combined with several well-known numerical methods for example finite element, (compact) finite difference and element free Galerkin methods. The POD method produces a new basis that keeps the most properties of the original data.

The POD approach has been studied by several researchers for example Xiao et. al [110] developed a novel non-intrusive reduced order model based on a RBF technique combined with the POD procedure for multiphase flows in porous media, Bistrian and Navon [13] presented an improved framework for dynamic mode decomposition based on the shallow water equations model reduction, Cao et. al [20] investigated a four-dimensional variational data assimilation (4DVAR) technique based on POD scheme to study a reduced gravity wave ocean model, Du and his co-workers [35, 36] derived a POD-based reduced-order model for the parabolized Navier-Stokes (PNS) equations, Luo and his co-authors [78] employed the POD algorithm for model reduction of mixed

finite element method for the nonstationary Navier-Stokes equations with some error estimates, Xiao et.al [111] developed a new reduced order model based upon POD idea to simulate the Navier-Stokes equations, a new nonlinear Petrov-Galerkin approach has been combined with POD reduced order modelling for the Navier-Stokes equations in [112, 113], Xiao and his co-workers [114] proposed two new non-intrusive reduced order models based upon POD. Finally Zhang and Xiang [126] proposed a fast element free Galerkin method based on POD bases for solving the transient heat conduction problems.

Wang et. al. [115] proposed two new closure models for the proper orthogonal decomposition reduced-order modeling of structurally dominated turbulent flows: the dynamic subgrid-scale model and the variational multiscale model. Authors of [117] investigated POD/DEIM model order reduction for the 2D Burgers equation based on the existing high fidelity implicit finite difference full model and coupled it with a Tikhonov regularization calibration for high Reynolds number.

1.4 The main objectives and organization of the paper

In this paper, we want to find a fast local meshless method based on the decrease computing time for solving shallow water equations in one- and two-dimensional cases. To reduce the used CPU time, we combine the proper orthogonal decomposition approach with a local meshless collocation technique based on the RBF-FD approach. The used algorithm employs an optimal shape parameter that it is taken from [15]. Also, the structure of this article is as follows:

- In Section 2, we explain the RBF-FD technique.
- In Section 3, we discuss on the conservation property of the numerical technique.
- In Section 4, the proper orthogonal decomposition idea is explained.
- In Section 5, we simulate the shallow water equations using the present method.
- Finally, a brief conclusion for the presented technique is written in Section 6.

2 Two bases in topic of meshless approximations

In the current paper, we introduce two bases to approximate an unknown function.

2.1 The Moving Kriging (MK) interpolation

The (MK) approach similar to moving least squares (MLS) approximation can be developed over any subdomain $\Omega_1 \subset \Omega$. The shape functions of moving kriging interpolation method unlike the shape functions of moving least squares approximation have the δ-Kronecker property. Thus using these shape functions the Dirichlet boundary condition can be applied directly. Also, the used CPU time for constructing the shape functions moving Kriging interpolation technique is less than the used CPU time for building the shape functions of moving least squares approximation. This section has been taken from [52, 130]. Let function $u_h(\mathbf{x})$ be the approximate solution of function $u(\mathbf{x})$ on the problem domain Ω. Over any subdomain Ω_x the local approximation is as follows

$$u^h(\mathbf{x}) = \sum_{j=1}^{m} p_j(\mathbf{x}) a_j + Z(\mathbf{x}) = \mathbf{p}^T(\mathbf{x})\mathbf{a} + \mathbf{Z}(\mathbf{x}), \tag{2.1}$$

where $p_j(x)$ for $j = 1, 2, \ldots, m$ are monomial basis function, a_j for $j = 1, 2, \ldots, m$ are monomial coefficient. We consider $Z(\mathbf{x})$ be the realization of a stochastic process with mean zero, variance σ^2, and non-zero covariance. The covariance matrix of $Z(\mathbf{x})$ is as follows [52, 130]

$$\operatorname{cov}\{Z(\mathbf{x}_i), Z(\mathbf{x}_j)\} = \sigma^2 \mathbf{R}\left[R(\mathbf{x}_i, \mathbf{x}_j)\right]. \tag{2.2}$$

In the above relation, $\mathbf{R}\left[R(\mathbf{x}_i, \mathbf{x}_j)\right]$ and $R(\mathbf{x}_i, \mathbf{x}_j)$ are the correlation matrix and the correlation function between any pair of nodes located at $\mathbf{x}_i$ and $\mathbf{x}_j$, respectively. A simple and frequently choice for selecting the correlation function is the following Gaussian function [52, 130]

$$R(\mathbf{x}_i, \mathbf{x}_j) = \exp(-\theta r_{ij}^2), \qquad r_{ij} = \|\mathbf{x}_i - \mathbf{x}_j\|, \tag{2.3}$$

and $\theta > 0$ represents a value of the correlation parameter used to fit the model. Now, implementing the best linear unbiased (BLUP) [52], Eq. (2.1) can be written as follows [52, 130]

$$u^h(\mathbf{x}) = \mathbf{p}^T(\mathbf{x})\eta + \mathbf{r}^T(\mathbf{x})\mathbf{R}^{-1}(\mathbf{u} - \mathbf{P}\eta), \tag{2.4}$$

in which

$$\eta = \left(\mathbf{P}^T\mathbf{R}^{-1}\mathbf{P}\right)^{-1}\mathbf{P}^T\mathbf{R}^{-1}\mathbf{u}. \tag{2.5}$$

In the following, we define some notations. The vector of the m known functions is as follows

$$\mathbf{p}(\mathbf{x}) = \begin{bmatrix} p_1(\mathbf{x}) & p_2(\mathbf{x}) & \ldots & p_m(\mathbf{x}) \end{bmatrix}^T, \tag{2.6}$$

and matrix of evaluated function values at set of nodes $x_1, x_2, \ldots, x_n$ is of the following form [52, 130]

$$\mathbf{P} = \begin{bmatrix} p_1(x_1) & p_2(x_1) & \ldots & p_m(x_1) \\ p_1(x_2) & p_2(x_2) & \ldots & p_m(x_2) \\ \vdots & \vdots & \ddots & \vdots \\ p_1(x_n) & p_2(x_n) & \ldots & p_m(x_n) \end{bmatrix}_{n\times m}. \tag{2.7}$$

The matrix of correlation is as follows

$$\mathbf{R}\left[R(\mathbf{x}_i, \mathbf{x}_j)\right] = \begin{bmatrix} 1 & R(\mathbf{x}_1, \mathbf{x}_2) & \ldots & R(\mathbf{x}_1, \mathbf{x}_n) \\ R(\mathbf{x}_2, \mathbf{x}_1) & 1 & \ldots & R(\mathbf{x}_2, \mathbf{x}_n) \\ \vdots & \vdots & \ddots & \vdots \\ R(\mathbf{x}_n, \mathbf{x}_1) & R(\mathbf{x}_n, \mathbf{x}_2) & \ldots & 1 \end{bmatrix}_{n\times n}, \tag{2.8}$$

and also the vector of correlation at set of nodes $x_1, x_2, \ldots, x_n$ is of the following form

$$\mathbf{r}(\mathbf{x}) = \begin{bmatrix} R(\mathbf{x}_1, \mathbf{x}) & R(\mathbf{x}_2, \mathbf{x}) & \ldots & R(\mathbf{x}_n, \mathbf{x}) \end{bmatrix}^T. \tag{2.9}$$

The matrices $\mathbf{A}$ and $\mathbf{B}$ are of the following form

$$\mathbf{A} = \left(\mathbf{P}^T\mathbf{R}^{-1}\mathbf{P}\right)^{-1}\mathbf{P}^T\mathbf{R}^{-1}, \tag{2.10}$$

$$\mathbf{B} = \mathbf{R}^{-1}(\mathbf{I} - \mathbf{P}\mathbf{A}), \tag{2.11}$$

where $\mathbf{I}$ is $n \times n$ identity matrix. Now, we write Eq. (2.4) as follows [52, 130]

$$u^h(\mathbf{x}) = \mathbf{p}^T(\mathbf{x})\mathbf{A}\mathbf{u} + \mathbf{r}^T(\mathbf{x})\mathbf{B}\mathbf{u}, \tag{2.12}$$

or

$$u^h(\mathbf{x}) = \left[\mathbf{p}^T(\mathbf{x})\mathbf{A} + \mathbf{r}^T(\mathbf{x})\mathbf{B}\right]\mathbf{u} = \sum_{k=1}^{n} \phi_k(\mathbf{x}) u_k = \varphi(\mathbf{x})\mathbf{u}, \tag{2.13}$$

where the shape functions of moving Kriging approach are as:

$$\varphi(\mathbf{x}) = \left(\mathbf{p}^T(\mathbf{x})\mathbf{A} + \mathbf{r}^T(\mathbf{x})\mathbf{B}\right)_j = [\phi_1, \phi_2, \ldots, \phi_n]^T. \tag{2.14}$$

2.2 The radial basis functions (RBFs) technique

In the current section, we explain the local RBF-DQ method thus at first we give some preliminaries for the radial basis function.

Definition 2.1. *[42, 105] A real valued continuous function $\phi \in \mathbb{R}^d \longrightarrow \mathbb{C}$ is positive definite if for all sets $X = \{x_1, \ldots, x_N\} \subset \mathbb{R}^d$ of distinct points and all vectors $\lambda \in \mathbb{R}^d$*

$$\lambda^T \phi \lambda = \sum_{i=1}^{N} \sum_{j=1}^{N} \lambda_i \lambda_j \phi(x_i - x_j) \geq 0. \tag{2.15}$$

Also, the function ϕ is called strictly positive definite on $\mathbb{R}^d$ if the quadratic form (2.15) is zero only for $\lambda = 0$.

We interpolate a continuous function $f : \mathbb{R}^d \longrightarrow \mathbb{R}$ on a set $X = \{x_1, \ldots, x_N\}$ with choosing the radial basis function for $\phi : \mathbb{R}^d \longrightarrow \mathbb{R}$ that is radial in the sense that $\phi(x) = \Psi(\|x\|)$, where $\|.\|$ is the usual Euclidean norm on $\mathbb{R}^d$ as we will explain it in the next section. Now, we assume ϕ to be strictly positive definite, then the interpolation function has the following form [42, 105]

$$\mathcal{I}(f(x)) = \sum_{i=1}^{N} \lambda_i \phi(x - x_i), \tag{2.16}$$

where $l = \begin{pmatrix} d+m-1 \\ m-1 \end{pmatrix}$. The basic problem is to find $N + l$ unknown coefficients λ_i in which N interpolation conditions are to the following form [42, 105]

$$\mathcal{I}(f(x_i)) = f_i, \qquad i = 1, \ldots, N. \tag{2.17}$$

It has proved that the interpolation matrix based on a strictly positive definite function is nonsingular [42, 105]. In the following, we mention some strictly positive functions:

1. **Gaussian:**

$$\phi(r) = \exp\left(-(\varepsilon r)^2\right), \tag{2.18}$$

2. **Linear generalized IMQ:**

$$\phi(r) = \frac{2 - (\varepsilon r)^2}{\left(1 + (\varepsilon r)^2\right)^4}. \tag{2.19}$$

3. **Linear Laguerre-Gaussian:**

$$\phi(r) = \exp\left(-(\varepsilon r)^2\right)\left(2 - (\varepsilon r)^2\right), \tag{2.20}$$

4. **Quadratic Laguerre-Gaussian:**

$$\phi(r) = \exp\left(-(\varepsilon r)^2\right)\left(3 - 3(\varepsilon r)^2 + \frac{1}{2}(\varepsilon r)^4\right). \tag{2.21}$$

In the current paper, we employ the **Gaussian** shape function that its interpolation matrix is non-singular.

2.3 Applying a suitable shape parameter

The accuracy of many schemes for interpolating scattered data with radial basis functions and to solve partial differential equations using meshfree methods based on radial basis functions depends on a shape parameter c, of the radial basis function [75, 86]. Thus, in this paper, we use an algorithm to obtain an optimal shape parameter that has been proposed by Sarra [87]. The used parameters

Algorithm 1 An optimal shape parameter [87]

```
κ = 0
while κ < κ_min, κ > κ_max do
    Produce interpolation matrix A
    [U, S, V] = svd(A)
    κ = σ_max / σ_min
    if κ < κ_min then
        c = c − c_Increment
    else
        c = c − c + Increment
    end if
end while
```

in the above code are as follows

1. **A** is the interpolation matrix
2. σ_{max} and σ_{min} are largest and lowest singular values of SVD decomposition, respectively.
3. $\mathrm{c_{Increment}} = \frac{1}{\mathrm{N}}$ in which N is total points in the cosidered domain.
4. $\kappa_{\min} = 1e+2$ and $\kappa_{\max} = 1e+4$.

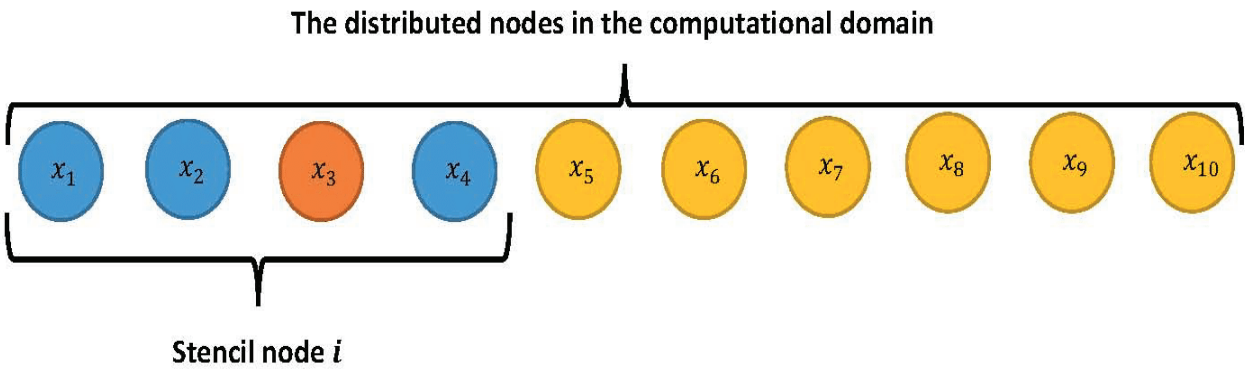

Figure 1: The used stencil in one-dimensional case

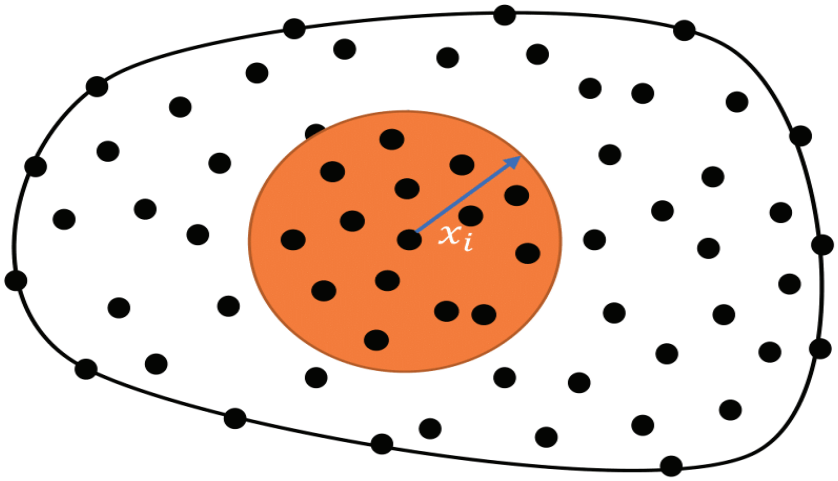

Figure 2: The used stencil in two-dimensional case

2.4 The RBF-FD procedure

In this section, we explain the local collocation meshless method based on an arbitrary shape function. As is well-known the local interpolation procedure is as follows [45, 46]

$$\mathcal{E}_m f(\vec{x}) = \sum_{j \in \mathcal{I}_i} \vec{\beta}_j \psi \left(\|\vec{x} - \vec{y}_j\| \right), \tag{2.22}$$

in which

1. $\vec{y}$ is set of N centers
2. $\mathcal{I}_i$ is set of nodes that are into the stencil of i^{th} node
3. $\vec{\beta}$ is the unknown weights that must be computed.

Also, the unknown weight can be calculated using the following interpolation conditions [45, 46]

$$\mathcal{E}_m f(\vec{x}_j) = f(\vec{x}_j). \tag{2.23}$$

Eq. (2.23) is equal to the following linear system of equations

$$\mathbf{A}\vec{\beta} = \mathbf{f}, \tag{2.24}$$

in which

$$\mathbf{f} = \left[f(\vec{x}_1), f(\vec{x}_2), \ldots, f(\vec{x}_{|\mathcal{I}_i|})\right], \qquad \mathbf{B}_{jk} = \psi\left(\|\vec{x}_j - \vec{x}_k\|_2\right), \quad j,k \in \mathcal{I}_i.$$

A local RBFs operator (including local derivatives or etc) can be obtained as follows [45, 46]

$$\mathcal{L}f(\vec{x}) = \sum_{j\in\mathcal{I}_i} \vec{\beta}_j \mathcal{L}\psi\left(\|\vec{x} - \vec{y}_j\|_2\right). \tag{2.25}$$

The above relation may be compacted in the following form

$$\mathcal{L}f(x) = \vec{h}^T\vec{\beta}, \tag{2.26}$$

where

$$(h)_i = \psi\left(\|x - y_i\|_2\right), \qquad i \in \mathcal{I}_i. \tag{2.27}$$

Eqs. (2.24) and (2.26) yield

$$\mathcal{L}f(\vec{x})|_{\mathcal{I}_i} = \left(\vec{h}^T\mathbf{B}^{-1}\right)\mathbf{f}\Big|_{\mathcal{I}_i} = (\vec{w}_i)\,\mathbf{f}, \tag{2.28}$$

in which $\vec{w}_i$ is the stencil weights at the shape function center i [45, 46].

2.5 One dimensional case

We explain implementing the RBF-FD method on the 1D shallow water equation and for other models in the current paper there is a similar way. Now, we consider the following model

$$\begin{cases} \dfrac{\partial h}{\partial t} + \dfrac{\partial\,(uh)}{\partial x} = 0, \\ \dfrac{\partial\,(uh)}{\partial t} + \dfrac{\partial\,(hu^2)}{\partial x} + \dfrac{g}{2}\dfrac{\partial\,(h^2)}{\partial x} = -ghB_x(x), \end{cases} \tag{2.29}$$

in which $h = h(x,t)$ is the water depth, $u = u(x,t)$ is the fluid horizontal velocity, g is the acceleration due to gravity and $B(x)$ is the bed depth from a fixed reference level, see Figure 3. Also, $B_x(x) = \dfrac{dB(x)}{dx}$. According to Eq. (2.28), the approximation solution is

$$h(x,t)|_{\mathcal{I}_i} = \sum_{j=1}^{n_s} w_j h_j(t), \tag{2.30}$$

also, the approximation first-order derivative is

$$\left.\frac{\partial h(x,t)}{\partial x}\right|_{\mathcal{I}_i} = \sum_{j=1}^{n_s} w_j^x h_j(t), \tag{2.31}$$

in which w_i^x is the weighting-coefficient matrix of the first-order derivative in x direction. Similarly,

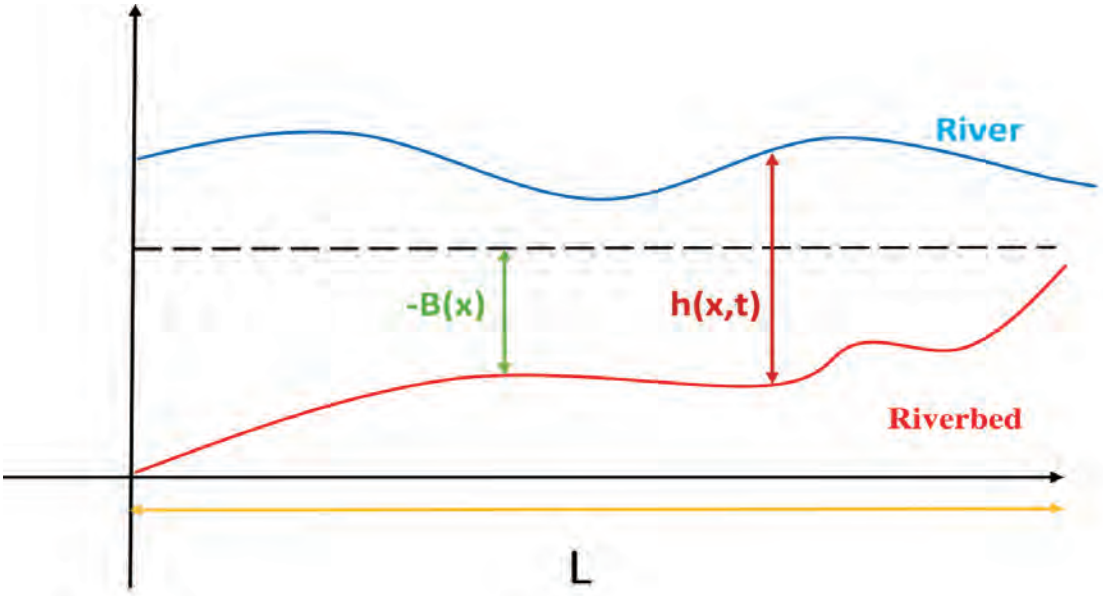

Figure 3: Shallow water variables

for v component there are the same approximations

$$uh(x,t)|_{\mathcal{I}_i} = \sum_{j=1}^{n_s} w_j uh_i(t), \qquad \left.\frac{\partial uh(x,t)}{\partial x}\right|_{\mathcal{I}_i} = \sum_{j=1}^{n_s} w_j^x uh_j(t). \tag{2.32}$$

Substituting Eqs. (2.30)-(2.45) in Eq. (2.41) yields

$$\begin{cases} \dfrac{dh_i(t)}{dt} + \displaystyle\sum_{j=1}^{\#\mathcal{I}_i} w_j^x (uh)_j(t) = 0, \qquad i = 1, 2, \ldots, N, \\ \dfrac{d(uh)_i(t)}{dt} + \displaystyle\sum_{j=1}^{\#\mathcal{I}_i} w_j^x (u^2 h)_j(t) + \frac{g}{2} \sum_{j=1}^{\#\mathcal{I}_i} w_j^x (h^2)_j(t) = -g h_i(t) B_x(x_i), \qquad i = 1, 2, \ldots, N, \end{cases} \tag{2.33}$$

where by collocating the nodes we obtain the following system of ordinary differential equations (ODEs)

$$\begin{cases} \dfrac{d\overrightarrow{\mathbf{h}}(t)}{dt} + \mathbf{D}_x \overrightarrow{\mathbf{uh}}(t) = \mathbf{0}, \\ \dfrac{d\overrightarrow{\mathbf{uh}}(t)}{dt} + \mathbf{D}_x \overrightarrow{\mathbf{u^2 h}}(t) + \dfrac{g}{2} \mathbf{D}_x \overrightarrow{\mathbf{h^2}}(t) = -g \overrightarrow{\mathbf{h}} .* \overrightarrow{\mathbf{B}}_x, \end{cases} \tag{2.34}$$

in which

$$\mathbf{h}(t) \;=\; \begin{bmatrix} h_1(t) & h_2(t) & \ldots & h_{N-1}(t) & h_N(t) \end{bmatrix},$$

$$\mathbf{u}(t) = \left[\begin{array}{ccccc} u_1(t) & u_2(t) & \dots & u_{N-1}(t) & u_N(t) \end{array}\right],$$

$$\mathbf{uh}(t) = \mathbf{u}(t).*\mathbf{h}(t),$$

$$\mathbf{B}_x = \left[\begin{array}{ccccc} B_x(x_1) & B_x(x_2) & \dots & B_x(x_{N-1}) & B_x(x_N) \end{array}\right],$$

Also, the structure of matrix $\mathbf{D}_x$ will be different based on the number of points in each sub-domain for example when we consider three points in each sub-domain then $\mathbf{D}_x$ will be a tridiagonal matrix as follows

$$\mathbf{D}_x = \left[\begin{array}{ccccccc} w_1^x & w_2^x & 0 & 0 & \dots & 0 & 0 \\ w_1^x & w_2^x & w_3^x & 0 & \dots & 0 & 0 \\ 0 & w_2^x & w_3^x & w_4^x & 0 & \dots & 0 \\ 0 & 0 & \ddots & \ddots & \ddots & \ddots & \vdots \\ \vdots & \vdots & \ddots & \ddots & \ddots & \ddots & 0 \\ 0 & 0 & \dots & 0 & w_{N-3}^x & w_{N-2}^x & w_{N-1}^x \\ 0 & \dots & \dots & 0 & 0 & w_{N-2}^x & w_{N-1}^x \end{array}\right],$$

or if we have five points in each sub-domain then $\mathbf{D}_x$ will be a five-diagonal matrix and the same way for other cases.

2.6 Hyperviscosity

The differentiation matrix of convective operator is as follows

$$D = \alpha_1 \frac{\partial}{\partial x} + \alpha_2 \frac{\partial}{\partial y}, \tag{2.35}$$

in which α_1 and α_2 are functions of fluid velocity. The convective operator that has been discretized using the RBF-FD technique, has eigenvalues in the right half-plane and thus the used method is unstable [45, 46]. As is mentioned in [14, 46] the stabilization of the RBF-FD procedure can be obtained by applying a hyperviscosity filter to Eq. (2.35). Consider the Gaussian RBFs as

$$\phi(r) = e^{-(\varepsilon r)^2}, \tag{2.36}$$

then the hyperviscosity can be simplified to

$$\Delta^k \phi(r) = \varepsilon^{2k} p_k(r) \phi(r), \tag{2.37}$$

in which k is the order of the Laplacian and $p_k(r)$ are multiples of generalized Laguerre polynomials that are generated recursively [14, 46].

In the case of parabolic PDEs, hyperviscosity is added as a filter to the right hand side of the model. For example, the main equation can be changed as follows

$$\frac{\partial u}{\partial t} = -Du + Hu, \tag{2.38}$$

in which D is the convective operator and H is the hyperviscosity filter operator. In fact, the hyperviscosity shifts all the eigenvalues of D to the left half of the complex plane [14, 46]. Also, the mentioned shift can be controlled by p the order of the Laplacian and a scaling parameter β_c as

$$H = \beta\Delta^p = \beta_c N^{-p}\Delta^p. \tag{2.39}$$

Given a choice of ε, it was found experimentally that $\beta = \beta_c N^{-p}$ provides stability and good accuracy for all values of N considered here. For example, we consider Eq. (2.41) as follows

$$\begin{cases} \dfrac{\partial h}{\partial t} + \dfrac{\partial\,(uh)}{\partial x} + N_n^p \dfrac{\partial^2 h}{\partial x^2} = 0, \\ \dfrac{\partial\,(uh)}{\partial t} + \dfrac{\partial\,(hu^2)}{\partial x} + \dfrac{g}{2}\dfrac{\partial\,(h^2)}{\partial x} = -ghB_x(x), \end{cases} \tag{2.40}$$

in which N_n is the number of nodes that are scattered in the computational domain and also in the computational results we consider $p = -0.68$.

Furthermore, it must be mentioned that to solve the conservation laws problems there is another approach to overcome the ill-posed problem. This approach is based on the upwinding approach in meshless method. The interested readers can find more details in [2].

2.7 Two-dimensional case

Implementing the RBF-FD method for the 2D shallow water equations is similar. Thus, we select one of them and explain the RBF-FD method for that particular model. Now, let the shallow water equation be

$$\begin{cases} \dfrac{\partial h}{\partial t} + \dfrac{\partial(hu)}{\partial x} + \dfrac{\partial(hv)}{\partial y} = \gamma\left(\dfrac{\partial^2 h}{\partial x^2} + \dfrac{\partial^2 h}{\partial y^2}\right), \\ \dfrac{\partial u}{\partial t} + \dfrac{u\partial u}{\partial x} + \dfrac{v\partial u}{\partial y} - fv = \theta\left(\dfrac{\partial^2 u}{\partial x^2} + \dfrac{\partial^2 u}{\partial y^2}\right) - g\dfrac{\partial(h+w_b)}{\partial x} - c_D\dfrac{u\sqrt{u^2+v^2}}{h}, \\ \dfrac{\partial v}{\partial t} + \dfrac{u\partial v}{\partial x} + \dfrac{v\partial v}{\partial y} + fu = \theta\left(\dfrac{\partial^2 v}{\partial x^2} + \dfrac{\partial^2 v}{\partial y^2}\right) - g\dfrac{\partial(h+w_b)}{\partial y} - c_D\dfrac{v\sqrt{u^2+v^2}}{h}, \\ \dfrac{\partial \phi}{\partial t} + \dfrac{u\partial \phi}{\partial x} + \dfrac{v\partial \phi}{\partial y} = \varepsilon\left(\dfrac{\partial^2 \phi}{\partial x^2} + \dfrac{\partial^2 \phi}{\partial y^2}\right) + \alpha\dfrac{\eta(\phi-\phi^*)}{h}, \\ \dfrac{\partial h_b}{\partial t} + g_b\left(\dfrac{\partial u}{\partial x} + \dfrac{\partial v}{\partial y}\right) = \alpha\dfrac{\eta(\phi-\phi^*)}{\rho}, \end{cases} \tag{2.41}$$

in which for the above model, we have [77, 125]:

- γ and θ are two coefficients of viscosity
- (u, v) is the vector of velocity

- $h = h^* - h_b$ is the water depth that h^* is the surface height and h_b is the height of the bed
- f is the Coriolis constant
- g is the gravitational constant
- c_D is the coefficient of bottom drag
- ε is the diffusion coefficient of sand
- ξ is the falling speed of suspended sediment particles
- ϕ is the concentration of sediment in water
- ϕ^* is the capacity for sediment transport in the bottom bed that is defined as

$$\phi^* = K\left[\frac{(u^2+v^2)^{\frac{3}{2}}}{g\xi h}\right]^m, \tag{2.42}$$

- ρ is the density of dry sand
- g_b a given empirical function that is defined as

$$g_b = \left(\Gamma(u^2+v^2)\right)^{\frac{3}{2}} w^p d^q \left[1 - \frac{v_c}{\sqrt{u^2+v^2}}\right], \tag{2.43}$$

- v_c is the velocity of sediment mass transport
- d is the diameter of sediment
- K, m, Γ, p and q are all empirical constants.

Also, the employed boundary conditions are as follows

$$\begin{cases} h(x,y,t) = h_0(x,y,t), \qquad u(x,y,t) = u_0(x,y,t), \qquad h_b(x,y,t) = h_{b0}(x,y,t), \\ v(x,y,t) = v_0(x,y,t), \qquad \phi(x,y,t) = \phi_0(x,y,t), \qquad (x,y,t) \in \partial\Omega \times (0,T). \end{cases}$$

According to Eq. (2.28), the approximation first-order derivative is

$$\left.\frac{\partial h(x,t)}{\partial x}\right|_{I_i} = \sum_{j=1}^{n_s} w_j^x h_j(t), \tag{2.44}$$

in which w_j^x is the weighting-coefficient matrix of the first-order derivative in x direction. Similarly, for other components there are the same approximations

$$\begin{aligned} \left.\frac{\partial u(x,t)}{\partial x}\right|_{I_i} &= \sum_{j=1}^{n_s} w_j^x u_j(t), & \left.\frac{\partial v(x,t)}{\partial x}\right|_{I_i} &= \sum_{j=1}^{n_s} w_j^x v_j(t), \\ \left.\frac{\partial \phi(x,t)}{\partial x}\right|_{I_i} &= \sum_{j=1}^{n_s} w_j^x \phi_j(t), & \left.\frac{\partial h_b(x,t)}{\partial x}\right|_{I_i} &= \sum_{j=1}^{n_s} w_j^x h_{bj}(t). \end{aligned} \tag{2.45}$$

Also, w_j^y is the weighting-coefficient matrix of the first-order derivative in y direction

$$\begin{aligned} \left.\frac{\partial u(x,t)}{\partial y}\right|_{I_i} &= \sum_{j=1}^{n_s} w_j^y u_j(t), & \left.\frac{\partial v(x,t)}{\partial y}\right|_{I_i} &= \sum_{j=1}^{n_s} w_j^y v_j(t), \\ \left.\frac{\partial \phi(x,t)}{\partial y}\right|_{I_i} &= \sum_{j=1}^{n_s} w_j^y \phi_j(t), & \left.\frac{\partial h_b(x,t)}{\partial y}\right|_{I_i} &= \sum_{j=1}^{n_s} w_j^y h_{bj}(t), \end{aligned} \tag{2.46}$$

and w_j^{xx} is the weighting-coefficient matrix of the second-order derivative in x direction

$$\begin{aligned} \left.\frac{\partial^2 u(x,t)}{\partial x^2}\right|_{I_i} &= \sum_{j=1}^{n_s} w_j^{xx} u_j(t), & \left.\frac{\partial^2 v(x,t)}{\partial x^2}\right|_{I_i} &= \sum_{j=1}^{n_s} w_j^{xx} v_j(t), \\ \left.\frac{\partial^2 \phi(x,t)}{\partial x^2}\right|_{I_i} &= \sum_{j=1}^{n_s} w_j^{xx} \phi_j(t), & \left.\frac{\partial^2 h_b(x,t)}{\partial x^2}\right|_{I_i} &= \sum_{j=1}^{n_s} w_j^{xx} h_{bj}(t), \end{aligned} \tag{2.47}$$

and so w_j^{yy} is the weighting-coefficient matrix of the second-order derivative in y direction

$$\begin{aligned} \left.\frac{\partial^2 u(x,t)}{\partial y^2}\right|_{I_i} &= \sum_{j=1}^{n_s} w_j^{yy} u_j(t), & \left.\frac{\partial^2 v(x,t)}{\partial y^2}\right|_{I_i} &= \sum_{j=1}^{n_s} w_j^{yy} v_j(t), \\ \left.\frac{\partial^2 \phi(x,t)}{\partial y^2}\right|_{I_i} &= \sum_{j=1}^{n_s} w_j^{yy} \phi_j(t), & \left.\frac{\partial^2 h_b(x,t)}{\partial y^2}\right|_{I_i} &= \sum_{j=1}^{n_s} w_j^{yy} h_{bj}(t). \end{aligned} \tag{2.48}$$

Thus, Eq. (2.41) can be written as follows

$$\begin{aligned} \frac{dh_i}{dt} + u_i \sum_{j=1}^{ns} w_j^x h_j(t) + h_i \sum_{j=1}^{ns} w_j^x u_j(t) + h_i \sum_{j=1}^{ns} w_j^x v_j(t) \\ + v_i \sum_{j=1}^{ns} w_j^x h_j(t) = \gamma \left(\sum_{j=1}^{ns} w_j^{xx} h_j(t) + \sum_{j=1}^{ns} w_j^{yy} h_j(t) \right), \end{aligned} \tag{2.49}$$

$$\frac{du_i(t)}{dt} + u_i(t)\sum_{j=1}^{n_s} w_j^x u_j(t) + v_i(t)\sum_{j=1}^{n_s} w_j^x u_j(t) - f_i(t)v_i(t)$$

$$= \theta\left(\sum_{j=1}^{n_s} w_j^{xx} u_j(t) + \sum_{j=1}^{n_s} w_j^{yy} u_j(t)\right) - g\left[\sum_{j=1}^{n_s} w_j^x h_j(t) + \sum_{j=1}^{n_s} w_j^x h_{bj}(t)\right] - c_D\frac{u_i(t)\sqrt{u_i^2(t)+v_i^2(t)}}{h_i(t)}, \tag{2.50}$$

$$\frac{dv_i(t)}{dt} + u_i(t)\sum_{j=1}^{n_s} w_j^x v_j(t) + v_i(t)\sum_{j=1}^{n_s} w_j^x v_j(t) + f u_i(t)$$

$$= \theta\left(\sum_{j=1}^{n_s} w_j^{xx} v_j(t) + \sum_{j=1}^{n_s} w_j^{yy} v_j(t)\right) - g\left[\sum_{j=1}^{n_s} w_j^x h_j(t) + \sum_{j=1}^{n_s} w_j^x h_{bj}(t)\right] - c_D\frac{v_i(t)\sqrt{u_i^2(t)+v_i^2(t)}}{h_i(t)}, \tag{2.51}$$

$$\frac{d\phi_i(t)}{dt} + u_i\sum_{j=1}^{n_s} w_j^x \phi_j(t) + v_i\sum_{j=1}^{n_s} w_j^y \phi_j(t) = \varepsilon\left(\sum_{j=1}^{n_s} w_j^{xx}\phi_j(t) + \sum_{j=1}^{n_s} w_j^{yy}\phi_j(t)\right) + \alpha\frac{\eta(\phi_i(t)-\phi^*)}{h_i(t)}, \tag{2.52}$$

$$\frac{dh_{bi}(t)}{dt} + g_b\left(\sum_{j=1}^{n_s} w_j^x u_j(t) + \sum_{j=1}^{n_s} w_j^y v_j(t)\right) = \alpha\frac{\eta(\phi_i(t)-\phi^*)}{\rho}, \tag{2.53}$$

for $i = 1, 2, \ldots, N$. Now, the matrix-vector form of the above equations is

$$\frac{d\mathbf{h}(t)}{dt} + \mathbf{u}(t)(\mathbf{D}_x\mathbf{h}(t)) + \mathbf{h}(t)\,(\mathbf{D}_x\mathbf{u}(t)) + \mathbf{h}(t)\,(\mathbf{D}_y\mathbf{v}(t)) + \mathbf{v}(t)\,(\mathbf{D}_y\mathbf{h}(t)) = \gamma\left[\mathbf{D}_{xx}\mathbf{h}(t) + \mathbf{D}_{yy}\mathbf{h}(t)\right], \tag{2.54}$$

$$\frac{d\mathbf{u}(t)}{dt} + \mathbf{u}(t)\,(\mathbf{D}_x\mathbf{u}(t)) + \mathbf{v}(t)\,(\mathbf{D}_y\mathbf{u}(t)) - f\mathbf{v}(t)$$

$$= \theta\left[\mathbf{D}_{xx}\mathbf{u}(t) + \mathbf{D}_{yy}\mathbf{u}(t)\right] - g\left[\mathbf{D}_x\mathbf{h}(t) + \mathbf{D}_x\mathbf{h}_b(t)\right] - c_D\frac{\mathbf{u}(t).*\sqrt{\mathbf{u^2}(t)+\mathbf{v^2}(t)}}{\mathbf{h}(t)}, \tag{2.55}$$

$$\frac{d\mathbf{v}(t)}{dt} + \mathbf{u}(t)\,(\mathbf{D}_x\mathbf{v}(t)) + \mathbf{v}(t)\,(\mathbf{D}_y\mathbf{v}(t)) - f\mathbf{u}(t)$$

$$= \theta\left[\mathbf{D}_{xx}\mathbf{v}(t) + \mathbf{D}_{yy}\mathbf{v}(t)\right] - g\left[\mathbf{D}_x\mathbf{h}(t) + \mathbf{D}_x\mathbf{h}_b(t)\right] - c_D\frac{\mathbf{v}(t).*\sqrt{\mathbf{u}^2(t)+\mathbf{v}^2(t)}}{\mathbf{h}(t)}, \tag{2.56}$$

$$\frac{d\boldsymbol{\phi}(t)}{dt} + \mathbf{u}(t)\,(\mathbf{D}_x\boldsymbol{\phi}(t)) + \mathbf{v}(t)\,(\mathbf{D}_y\boldsymbol{\phi}(t)) = \varepsilon\left[\mathbf{D}_{xx}\boldsymbol{\phi}(t) + \mathbf{D}_{yy}\boldsymbol{\phi}(t)\right] + \alpha\frac{\eta * (\boldsymbol{\phi}(t)-\boldsymbol{\phi}^*)}{\mathbf{h}(t)}, \tag{2.57}$$

$$\frac{d\mathbf{h}_b(t)}{dt} + g_b\left[\mathbf{D}_x\mathbf{u}(t) + \mathbf{D}_y\mathbf{v}(t)\right] = \alpha\frac{\eta * (\phi(t)-\phi^*)}{\rho}. \tag{2.58}$$

Also, the above relations may be rewritten as

$$\begin{aligned}
\frac{d\mathbf{h}(t)}{dt} + G_1(\mathbf{h},\mathbf{u},\mathbf{v}) &= \gamma\left[\mathbf{D}_{xx}\mathbf{h}(t) + \mathbf{D}_{yy}\mathbf{h}(t)\right], \\
\frac{d\mathbf{u}(t)}{dt} + G_2(\mathbf{h},\mathbf{u},\mathbf{v}) - f\mathbf{v}(t) &= \theta\left[\mathbf{D}_{xx}\mathbf{u}(t) + \mathbf{D}_{yy}\mathbf{u}(t)\right] - g\left[\mathbf{D}_x\mathbf{h}(t) + \mathbf{D}_x\mathbf{h}_b(t)\right], \\
\frac{d\mathbf{v}(t)}{dt} + G_3(\mathbf{h},\mathbf{u},\mathbf{v}) - f\mathbf{u}(t) &= \theta\left[\mathbf{D}_{xx}\mathbf{v}(t) + \mathbf{D}_{yy}\mathbf{v}(t)\right] - g\left[\mathbf{D}_x\mathbf{h}(t) + \mathbf{D}_x\mathbf{h}_b(t)\right], \\
\frac{d\boldsymbol{\phi}(t)}{dt} + G_4(\mathbf{h},\mathbf{u},\mathbf{v},\boldsymbol{\phi}) &= \varepsilon\left[\mathbf{D}_{xx}\boldsymbol{\phi}(t) + \mathbf{D}_{yy}\boldsymbol{\phi}(t)\right], \\
\frac{d\mathbf{h}_b(t)}{dt} + g_b\left[\mathbf{D}_x\mathbf{u}(t) + \mathbf{D}_y\mathbf{v}(t)\right] &= G_5(\mathbf{h},\phi),
\end{aligned} \tag{2.59}$$

in which

$$\begin{aligned}
G_1(\mathbf{h},\mathbf{u},\mathbf{v}) &= \mathbf{u}(t)\left(\mathbf{D}_x\mathbf{h}(t)\right) + \mathbf{h}(t)\left(\mathbf{D}_x\mathbf{u}(t)\right) + \mathbf{h}(t)\left(\mathbf{D}_y\mathbf{v}(t)\right) + \mathbf{v}(t)\left(\mathbf{D}_y\mathbf{h}(t)\right), \\
G_2(\mathbf{h},\mathbf{u},\mathbf{v}) &= \mathbf{u}(t)\left(\mathbf{D}_x\mathbf{u}(t)\right) + \mathbf{v}(t)\left(\mathbf{D}_y\mathbf{u}(t)\right) + c_D\frac{\mathbf{u}(t).*\sqrt{\mathbf{u^2}(t)+\mathbf{v^2}(t)}}{\mathbf{h}(t)}, \\
G_3(\mathbf{h},\mathbf{u},\mathbf{v}) &= \mathbf{u}(t)\left(\mathbf{D}_x\mathbf{v}(t)\right) + \mathbf{v}(t)\left(\mathbf{D}_y\mathbf{v}(t)\right) + c_D\frac{\mathbf{v}(t).*\sqrt{\mathbf{u}^2(t)+\mathbf{v}^2(t)}}{\mathbf{h}(t)}, \\
G_4(\mathbf{h},\mathbf{u},\mathbf{v},\boldsymbol{\phi}) &= \mathbf{u}(t)\left(\mathbf{D}_x\boldsymbol{\phi}(t)\right) + \mathbf{v}(t)\left(\mathbf{D}_y\phi(t)\right) - \alpha\frac{\eta*(\boldsymbol{\phi}(t)-\boldsymbol{\phi}^*)}{\mathbf{h}(t)}, \\
G_5(\mathbf{h},\boldsymbol{\phi}) &= \alpha\frac{\eta*(\boldsymbol{\phi}(t)-\boldsymbol{\phi}^*)}{\rho}.
\end{aligned} \tag{2.60}$$

As is clear system (2.59) is a semi-discrete scheme based on the temporal direction. There are some numerical approach for solving differentiation equation (2.59) such as finite difference, Runge-Kutta methods, etc. At first, we apply the implicit Euler technique to discrete the nonlinear system of equation (2.59) and then the Newton method is employed to solve the algebraic nonlinear system of equations. For positive integer number N_t, let $\tau = \frac{T}{N_t}$ denote the step size of time variable t. So we define

$$t_n = n\tau \qquad , \qquad n = 0, 1, 2, ..., N_t.$$

Now, we define

$$\begin{aligned}
F_1(\mathbf{h}^n,\mathbf{u}^n,\mathbf{v}^n,\phi,\mathbf{h}_b^n) &= \mathbf{h}^n - \mathbf{h}^{n-1} + dtG_1(\mathbf{h}^n,\mathbf{u}^n,\mathbf{v}^n) - dt\gamma\left[\mathbf{D}_{xx}\mathbf{h}^n + \mathbf{D}_{yy}\mathbf{h}^n\right], \\
F_2(\mathbf{h}^n,\mathbf{u}^n,\mathbf{v}^n,\phi,\mathbf{h}_b^n) &= \mathbf{u}^n - \mathbf{u}^{n-1} + dtG_2(\mathbf{h}^n,\mathbf{u}^n,\mathbf{v}^n) - dtf\mathbf{v}^n \\
&- dt\theta\left[\mathbf{D}_{xx}\mathbf{u}^n + \mathbf{D}_{yy}\mathbf{u}^n\right] - dtg\left[\mathbf{D}_x\mathbf{h}^n + \mathbf{D}_x\mathbf{h}_b^n\right],
\end{aligned}$$

$$
\begin{aligned}
F_3(\mathbf{h}^n,\mathbf{u}^n,\mathbf{v}^n,\phi,\mathbf{h}_b^n) &= \mathbf{v}^n-\mathbf{v}^{n-1}+dtG_3(\mathbf{h}^n,\mathbf{u}^n,\mathbf{v}^n)-dtf\mathbf{u}^n(t)\\
&- dt\theta\left[\mathbf{D}_{xx}\mathbf{v}^n+\mathbf{D}_{yy}\mathbf{v}^n\right]-dtg\left[\mathbf{D}_x\mathbf{h}^n+\mathbf{D}_x{\mathbf{h}_b}^n\right],\\
F_4(\mathbf{w}^n,\mathbf{u}^n,\mathbf{v}^n,\phi,\mathbf{h}_b^n) &= \phi^n-\phi^{n-1}+dtG_4(\mathbf{w}^n,\mathbf{u}^n,\mathbf{v}^n,\phi^n)-dt\varepsilon\left[\mathbf{D}_{xx}\phi^n+\mathbf{D}_{yy}\phi^n\right],\\
F_5(\mathbf{h}^n,\mathbf{u}^n,\mathbf{v}^n,\phi,\mathbf{h}_b^n) &= \mathbf{h}_b^n-\mathbf{h}_b^{n-1}+dtg_b\left[\mathbf{D}_x\mathbf{u}^n+\mathbf{D}_y\mathbf{v}^n\right]-dtG_5(\mathbf{h}^n,\phi^n),
\end{aligned}
\tag{2.61}
$$

in which

$$
\begin{aligned}
G_1(\mathbf{h}^n,\mathbf{u}^n,\mathbf{v}^n) &= \mathbf{u}^n\left(\mathbf{D}_x\mathbf{h}^n\right)+\mathbf{h}^n\left(\mathbf{D}_x\mathbf{u}^n\right)+\mathbf{h}^n\left(\mathbf{D}_y\mathbf{v}^n\right)+\mathbf{v}^n\left(\mathbf{D}_y\mathbf{h}^n\right),\\
G_2(\mathbf{h}^n,\mathbf{u}^n,\mathbf{v}^n) &= \mathbf{u}^n\left(\mathbf{D}_x\mathbf{u}^n\right)+\mathbf{v}^n\left(\mathbf{D}_y\mathbf{u}^n\right)+c_D\frac{\mathbf{u}^n.*\sqrt{\left(\mathbf{u}^n\right)^2+\left(\mathbf{v}^n\right)^2}}{\mathbf{h}^n},\\
G_3(\mathbf{h}^n,\mathbf{u}^n,\mathbf{v}^n) &= \mathbf{u}^n\left(\mathbf{D}_x\mathbf{v}^n\right)+\mathbf{v}^n\left(\mathbf{D}_y\mathbf{v}^n\right)+c_D\frac{\mathbf{v}^n.*\sqrt{\left(\mathbf{u}^n\right)^2+\left(\mathbf{v}^n\right)^2}}{\mathbf{h}^n},\\
G_4(\mathbf{h}^n,\mathbf{u}^n,\mathbf{v}^n) &= \mathbf{u}^n\left(\mathbf{D}_x\boldsymbol{\phi}^n\right)+\mathbf{v}^n\left(\mathbf{D}_y\boldsymbol{\phi}^n\right)-\alpha\frac{\eta*(\boldsymbol{\phi}^n-\boldsymbol{\phi}^*)}{\mathbf{h}^n},\\
G_5(\mathbf{h}^n,\boldsymbol{\phi}^n) &= \alpha\frac{\eta*(\boldsymbol{\phi}^n-\boldsymbol{\phi}^*)}{\rho}.
\end{aligned}
\tag{2.62}
$$

Now, we can obtain a linear system of algebraic equations based on the Taylor series expansion at the k^{th} iteration

$$
J^k\begin{bmatrix}\delta\mathbf{h}_k^n\\ \delta\mathbf{u}_k^n\\ \delta\mathbf{v}_k^n\\ \delta\boldsymbol{\phi}_k^n\\ \delta(\mathbf{h}_b)_k^n\end{bmatrix}=-\begin{bmatrix}F_1\\F_2\\F_3\\F_4\\F_5\end{bmatrix}^k, \tag{2.63}
$$

where

$$
J^k\begin{bmatrix}F_{1w}&F_{1u}&F_{3v}&F_{4\phi}&F_{5w_b}\\F_{1w}&F_{2u}&F_{3v}&F_{4\phi}&F_{5w_b}\\F_{1w}&F_{2u}&F_{3v}&F_{4\phi}&F_{5w_b}\\F_{1w}&F_{2u}&F_{3v}&F_{4\phi}&F_{5w_b}\\F_{1w}&F_{2u}&F_{3v}&F_{4\phi}&F_{5w_b}\end{bmatrix}. \tag{2.64}
$$

By solving Eq. (2.63), we obtain

$$\begin{bmatrix} \mathbf{h}_{k+1}^n \\ \mathbf{u}_{k+1}^n \\ \mathbf{v}_{k+1}^n \\ \boldsymbol{\phi}_{k+1}^n \\ (\mathbf{h}_b)_{k+1}^n \end{bmatrix} = \begin{bmatrix} \mathbf{h}_k^n \\ \mathbf{u}_k^n \\ \mathbf{v}_k^n \\ \boldsymbol{\phi}_k^n \\ (\mathbf{h}_b)_k^n \end{bmatrix} + \begin{bmatrix} \delta\mathbf{h}_k^n \\ \delta\mathbf{u}_k^n \\ \delta\mathbf{v}_k^n \\ \delta\boldsymbol{\phi}_k^n \\ \delta(\mathbf{h}_b)_k^n \end{bmatrix}. \tag{2.65}$$

Also, using the following condition the iterative process can be finished

$$\left\| \begin{bmatrix} \delta\mathbf{h}_k^n \\ \delta\mathbf{u}_k^n \\ \delta\mathbf{v}_k^n \\ \delta\phi_k^n \\ \delta(\mathbf{h}_b)_k^n \end{bmatrix} \right\| \leq tol. \tag{2.66}$$

3 A conservation property (C-property)

The space derivative discretization of the source term in the shallow water equations leads to numerical artificial waves [8]. The interested readers, to obtain more details on C-property can refer to [8]. Here, have followed and have used informations given in [3] to check the C-property.

Let the shallow water equations be as follows

$$\frac{\partial \mathbf{z}(x,t)}{\partial t} + \frac{\partial \mathbf{F}(\mathbf{z}(x,t))}{\partial x} = \mathbf{G}(x, \mathbf{z}(x,t)), \tag{3.1}$$

in which

$$\mathbf{z}(x,t) = \begin{bmatrix} h(x,t) \\ uh(x,t) \end{bmatrix}, \tag{3.2}$$

$$\mathbf{F}(\mathbf{z}(x,t)) = \begin{bmatrix} p(x,t) \\ \dfrac{p^2(x,t)}{h(x,t)} + \dfrac{1}{2}gh^2(x,t) \end{bmatrix}, \tag{3.3}$$

$$\mathbf{G}(x, \mathbf{z}(x,t)) = \begin{bmatrix} 0 \\ -gh(x,t)B_x(x) \end{bmatrix}. \tag{3.4}$$

In the above formulations:

- $h(x,t)$ is the total height above the bottom of the channel,
- $u(x,t)$ the fluid velocity,
- $B(x)$ is the depth of the same point but from a fixed reference level.

Theorem 3.1. *The proposed numerical scheme has the C-property.*

Proof. Now, a numerical plane is said to satisfy the C-property for Eq. (3.1) if the condition [3]

$$\left(\overrightarrow{\mathbf{h}}\right)^n + \overrightarrow{\mathbf{B}}(x) = \overrightarrow{c} = \text{Constant}, \quad \mathbf{u}^n = 0, \tag{3.5}$$

holds for stationary flows at rest. As is said in [3], the treatment of source terms in (2.50), is reconstructed such that the condition (3.5) is preserved at the discretized level. According to conditions (3.5), Eq. (3.1) can be rewritten as follows

$$\frac{\partial}{\partial t}\begin{bmatrix} h(x,t) \\ 0 \end{bmatrix} + \frac{\partial}{\partial x}\begin{bmatrix} 0 \\ \frac{1}{2}gh^2(x,t) \end{bmatrix} = \begin{bmatrix} 0 \\ gh(x,t)B_x(x) \end{bmatrix}. \tag{3.6}$$

Also, applying implicit Euler difference method on (2.50) arrives at

$$\begin{cases} \left(\overrightarrow{\mathbf{h}}\right)^{n+1} = \left(\overrightarrow{\mathbf{h}}\right)^n - \tau \mathbf{D}_x\left(\overrightarrow{\mathbf{uh}}\right)^n, \\ \left(\overrightarrow{\mathbf{uh}}\right)^{n+1} = \left(\overrightarrow{\mathbf{uh}}\right)^n - \tau \mathbf{D}_x\left(\overrightarrow{\mathbf{u^2h}}\right)^n - \frac{\tau g}{2}\mathbf{D}_x\left(\overrightarrow{\mathbf{h^2}}\right)^n - \tau g\left(\overrightarrow{\mathbf{h}}\right)^n .* \overrightarrow{\mathbf{B}}_x. \end{cases} \tag{3.7}$$

Now, using condition (3.5) on system of equations (3.7), yields

$$\begin{cases} \left(\overrightarrow{\mathbf{h}}\right)^{n+1} = \left(\overrightarrow{\mathbf{h}}\right)^n, \\ \left(\overrightarrow{\mathbf{uh}}\right)^{n+1} = \left(\overrightarrow{\mathbf{uh}}\right)^n - \frac{\tau g}{2}\mathbf{D}_x\left(\overrightarrow{\mathbf{h^2}}\right)^n - \tau g\left(\overrightarrow{\mathbf{h}}\right)^n .* \overrightarrow{\mathbf{B}}_x. \end{cases} \tag{3.8}$$

If we want to have a stationary solution $\left(\overrightarrow{\mathbf{h}}\right)^{n+1} = \left(\overrightarrow{\mathbf{h}}\right)^n$ the sum of discretized flux gradient and source term in relation (3.8) should be equal to zero, in other word

$$-\frac{\tau g}{2}\mathbf{D}_x\left(\overrightarrow{\mathbf{h^2}}\right)^n = \tau g\left(\overrightarrow{\mathbf{h}}\right)^n .* \overrightarrow{\mathbf{B}}_x. \tag{3.9}$$

As is mentioned before, we have

$$\overrightarrow{\mathbf{B}}_x = \frac{d\overrightarrow{\mathbf{B}}(x)}{dx},$$

thus we can approximate it by the following form

$$\overrightarrow{\mathbf{B}}_x = \mathbf{D}_x\overrightarrow{\mathbf{B}}(x). \tag{3.10}$$

Also from condition (3.5), we have

$$\mathbf{D}_x\left(\overrightarrow{\mathbf{h}}\right)^n = -\mathbf{D}_x\overrightarrow{\mathbf{B}}(x). \tag{3.11}$$

Substituting Eq. (3.11) in (3.9), gives

$$\tau g\Big(\overrightarrow{\mathbf{h}}\Big)^n .* \Big(\mathbf{D}_x\Big(\overrightarrow{\mathbf{h}}\Big)^n\Big) = \frac{\tau g}{2}\mathbf{D}_x\Big(\overrightarrow{\mathbf{h}^2}\Big)^n = \tau g\Big(\overrightarrow{\mathbf{h}}\Big)^n .* \Big(\mathbf{D}_x\Big(\overrightarrow{\mathbf{h}}\Big)^n\Big). \tag{3.12}$$

Thus, the proposed method satisfies the C-property. □

Also, we will check the C-property in Test problem 1.

4 Proper orthogonal decomposition method

The POD technique has been studied by many researchers [23, 25, 41, 71, 84, 85, 96, 97, 110] and also is an active field for new research works. Let $\Phi = [\Phi_k(x, t_k)] \in \mathbb{R}^{n_{xy}\times n_k}$ be a set of snapshots that is obtained using the numerical solution at equally distributed time instances $t_{n_1}, t_{n_2}, \ldots, t_{n_k}$ in which n_k is the number of snapshots. It is possible that the obtained snapshots are linear dependence thus these are not suitable for a new basis. The POD basis can be derived based on the following strategies:

- Singular value decomposition (SVD) for $\Phi = [\Phi_k(x, t_k)]$,
- Eigenvalue decomposition for $\Phi\Phi^T \in \mathbb{R}^{n_{xy}\times n_{xy}}$,
- Eigenvalue decomposition for $\Phi^T\Phi \in \mathbb{R}^{n_{xy}\times n_{xy}}$.

Since the governing model is system of PDEs, we employ the corresponding POD basis vectors for them based on the snapshots of the solution for each variable separately. Here we just describe the applied procedure to build the POD basis for u component and also there is a similar way for other components. Let $n_k \ll n_{xy}$ then by solving the following eigenvalue problem

$$\Phi^T\Phi\hat{h}_i = \lambda_i\hat{h}_i, \qquad\qquad i = 1, 2, \ldots, n_k, \tag{4.1}$$

we can select an orthogonal basis of eigenvectors

$$\left\{\hat{h}_1, \hat{h}_2, \ldots, \hat{h}_{m_1}\right\}, \tag{4.2}$$

corresponding to the m_1 largest eigenvalue. Thus POD basis of the component u is as follows

$$B_h^{POD,i} = \frac{1}{\sqrt{\lambda_i}}\Phi\widehat{h}_i, \tag{4.3}$$

$$B_h^{POD} = \left[B_h^{POD,i}, \quad i = 1, 2, \ldots, m_1\right] \in \mathbb{R}^{n_{xy}\times m_1}. \tag{4.4}$$

Similarly, we can obtain the optimal POD basis for components u and v i.e. $B_u^{POD} \in \mathbb{R}^{n_{xy}\times m_2}$ and $B_v^{POD} \in \mathbb{R}^{n_{xy}\times m_3}$. As is said in [103], these POD modes provide an optimal representation of the snapshot matrix, some information is inevitably lost in which we can get the following ratio [103]

$$I(m) = \left(\sum_{i=1}^{n_k}\lambda_i\right)^{-1}\sum_{i=1}^{m}\lambda_i. \tag{4.5}$$

According to the above explanations, the approximation of components $\mathbf{h}$, $\mathbf{u}$ and $\mathbf{v}$ and the POD bases can be related via the relation:

$$\mathbf{h}(t_n) \approx B_h^{POD}\mathbf{h}^{POD}(t_n), \tag{4.6}$$

$$\mathbf{u}(t_n) \approx B_u^{POD}\mathbf{u}^{POD}(t_n), \tag{4.7}$$

$$\mathbf{v}(t_n) \approx B_v^{POD}\mathbf{v}^{POD}(t_n), \tag{4.8}$$

in which $\mathbf{h}^{POD}(t_n) \in \mathbb{R}^{m_1}$, $\mathbf{u}^{POD}(t_n) \in \mathbb{R}^{m_2}$ and $\mathbf{v}^{POD}(t_n) \in \mathbb{R}^{m_3}$. The nonlinear term based on the POD reduced order model (POD-ROM) is

$$\begin{aligned}&\mathbf{G}_1^{POD}(\mathbf{h}^{POD}(t_n), \mathbf{u}^{POD}(t_n), \mathbf{v}^{POD}(t_n))\\ &\quad= \underbrace{\left(B_h^{POD}\right)^T}_{m_1\times n_{xy}}\underbrace{\mathbf{G}_1(B_u^{POD}\mathbf{h}^{POD}(t_n), B_v^{POD}\mathbf{u}^{POD}(t_n), B_v^{POD}\mathbf{v}^{POD}(t_n))}_{n_{xy}\times 1}.\end{aligned} \tag{4.9}$$

Also, for other nonlinear terms there are similar relations.

5 Numerical experiments

Here, several test problem are presented to show the accuracy and efficiency of the proposed technique. We performed our computations using **Matlab** 7 software on a Pentium IV, 2800 MHz CPU machine with 2 Gbyte of memory. It should be noted that the use of high number of points causes good results. Thus, in the numerical results we considered many nodes in proposed scheme. To show that the POD scheme approximates the full model, we employ the root mean square error (**RMSE**) and the correlation coefficient (**Corr**) to measure the difference between POD and full model as follows [117]

$$\mathbf{RMES}^n = \sqrt{\frac{\sum_{i=1}^{N}\left(U_i^{n(full)} - U_i^{n(POD)}\right)^2}{N}}, \tag{5.1}$$

$$\mathbf{Corr}^n = \frac{E(U^n - \mu_U)(U_0^n - -\mu_{U_0^n})}{\sigma_{U^n}\sigma_{U_0^n}}, \tag{5.2}$$

in which μ_U and $\mu_{U_0^n}$ are the given expected value and σ_{U^n} and $\sigma_{U_0^n}$ are the standard deviations.

In the current paper, we report (m, n_s) for all figures in which m is the employed POD modes and n_s is the used nodes into each sub-domain.

5.1 Test problem 1. (To check the C-property)

The main aim of the current example is to verify that the scheme preserves the exact C-property over a nonflat bottom. We select the following functions for the bottom topography [107]

$$B(x) = 5\exp\left(-\frac{2}{5}(x-5)^2\right), \tag{5.3}$$

and discontinuous case [3]

$$B(x) = \begin{cases} 0.2 - 0.05(x-10)^2, & 8 \le x \le 10, \\ 0, & o.w. \end{cases} \tag{5.4}$$

The initial data is the stationary solution

$$h + B = 10, \qquad hu = 0. \tag{5.5}$$

For this example, the steady state should be exactly preserved. We employ the proposed method

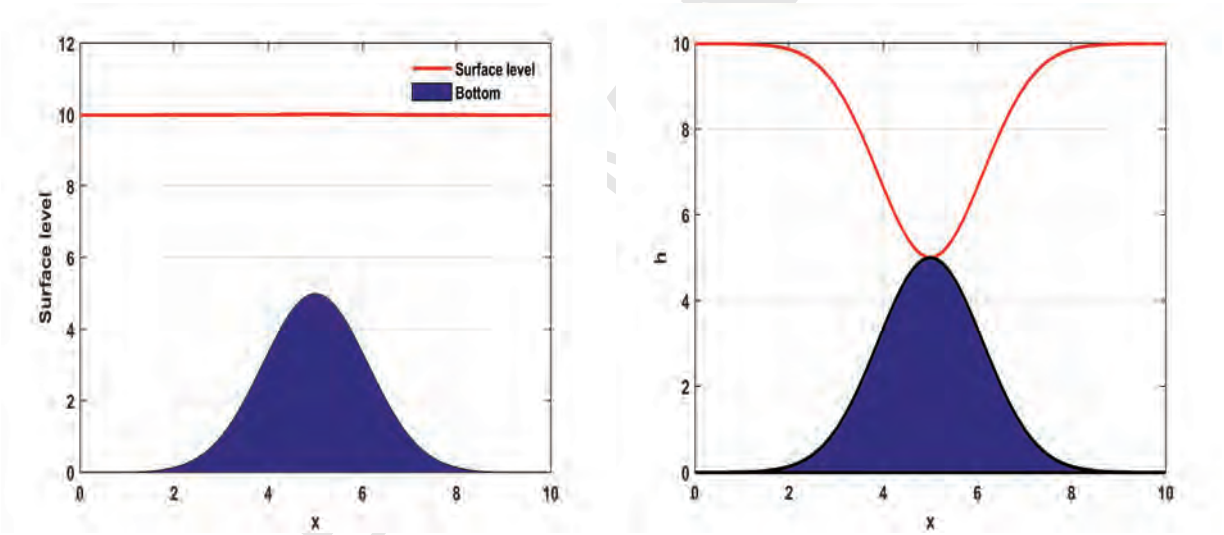

Figure 4: The surface level $h+B$ and the bottom B with $(m = 10, n_s = 21)$ and bottom topography (5.3) for the stationary flow over a smooth bump for Test problem 1.

with 400 collocation points at final time $T = 0.5$ and 10 POD modes. Figures 4 and 5 show the surface level $h + B$ and the bottom B. Table 1 contains the used CPU time(s) for Test problem 2. In order to illustrate that the exact C-property is preserved up to round-off error, we report L_∞ error related to water height h in Table 2 for RBF-FD and LMK methods.

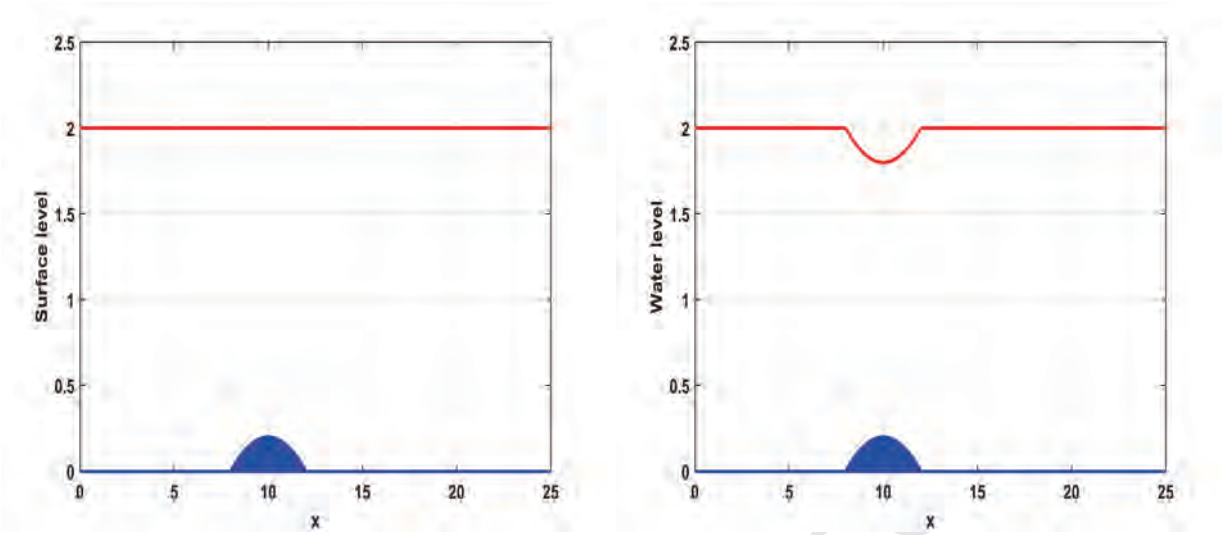

Figure 5: The surface level $h+B$ and the bottom B with $(m = 10, n_s = 21)$ and bottom topography (5.4) for the stationary flow over a smooth bump for Test problem 1.

Table 1: The used CPU time(s) for Test problem 1

		Computational Time	
Number of nodes	Number of POD bases	RBF-FD	POD
100	10	40	5.2
200	11	64	7.3
400	14	95	8.4
600	16	134	10.1
800	20	197	13.7

Table 2: Errors obtained for the stationary solution for Test problem 1

	bottom topography (5.3)		bottom topography (5.4)	
Number of nodes	RBF-FD	LMK	RBF-FD	LMK
200	4.2501×10^{-5}	3.2133×10^{-4}	5.1109×10^{-4}	6.7789×10^{-3}
400	6.0013×10^{-7}	7.4913×10^{-5}	8.9017×10^{-6}	3.1189×10^{-4}
600	1.0191×10^{-9}	1.6667×10^{-7}	6.3153×10^{-7}	5.8901×10^{-6}
1000	2.4598×10^{-11}	9.1001×10^{-9}	9.4530×10^{-10}	6.8002×10^{-8}

5.2 Test problem 2 (Hump of water problem):

We consider the one-dimensional shallow water equation as follows [66]

$$\begin{cases} \dfrac{\partial h}{\partial t} + \dfrac{\partial (uh)}{\partial x} = 0, \\ \dfrac{\partial (uh)}{\partial t} + \dfrac{\partial (hu^2)}{\partial x} + \dfrac{g}{2}\dfrac{\partial (h^2)}{\partial x} = 0, \end{cases} \tag{5.6}$$

with initial conditions

$$\begin{cases} h(x,0) = 1 + \dfrac{2}{5}\exp(-5x^2), \\ \\ uh(x,0) = 0, \end{cases} \tag{5.7}$$

and periodic boundary conditions

$$h(-5,t) = h(5,t), \qquad uh(-5,t) = uh(5,t). \tag{5.8}$$

We solve this example using local collocation methods based on radial basis functions and shape

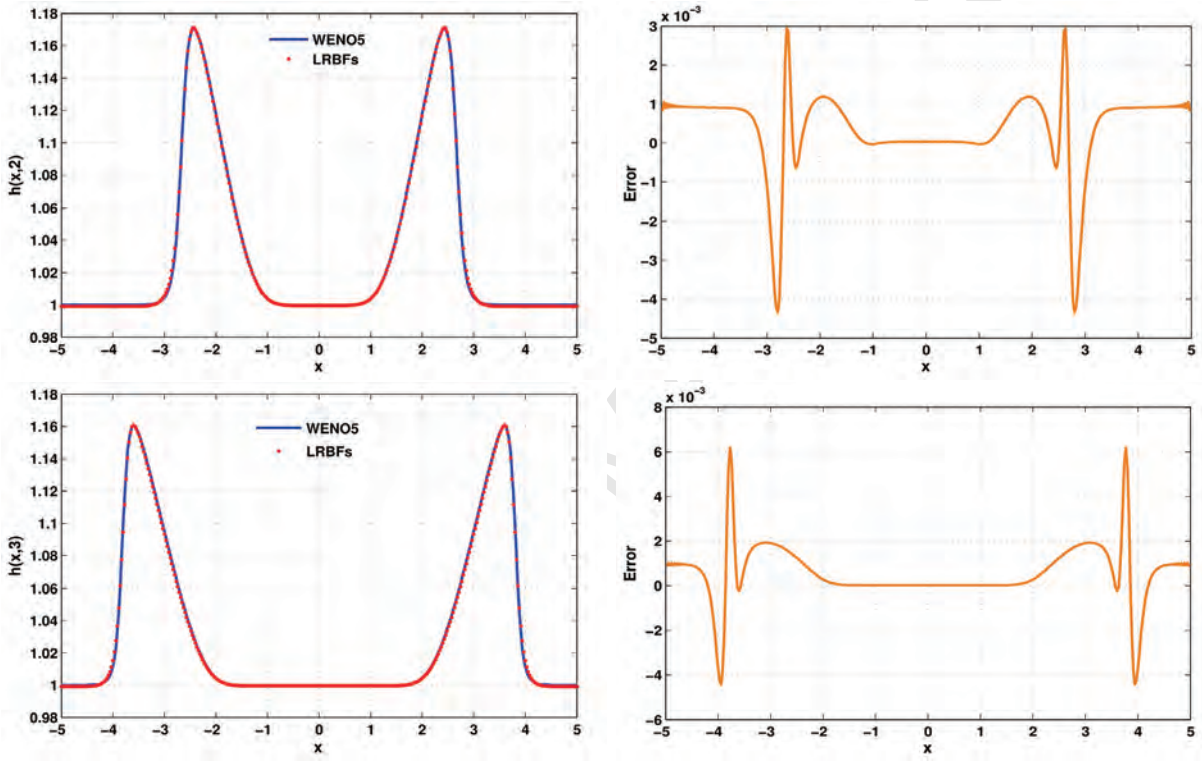

Figure 6: Graph of approximation solutions with $(m = 10, n_s = 11)$ based on the LRBF for Test problem 2.

functions of moving Kriging interpolation. For showing the validation of the obtained numerical results based on these two methods, we used the weighted essentially non-oscillatory (WENO) method [67]. Since Test problem 2 doesn't have the exact solution, we consider the obtained numerical results by WENO method [67] as an exact solution and then we compare them with the numerical schemes obtained in the current paper i.e. RBF-FD and LMK methods and also report the errors in Table 3 for Test problem 2.

Figure 6 shows the approximation solution using local radial basis functions collocation method with 350 total number nodes into computational domain and 90 nodes into each stencil and also we set $dt = 10^{-3}$ in two final times $T = 2$ (up figures) and $T = 3$ (down figures). In the current example, let the obtained numerical results using the WENO method [67] be as an exact solution

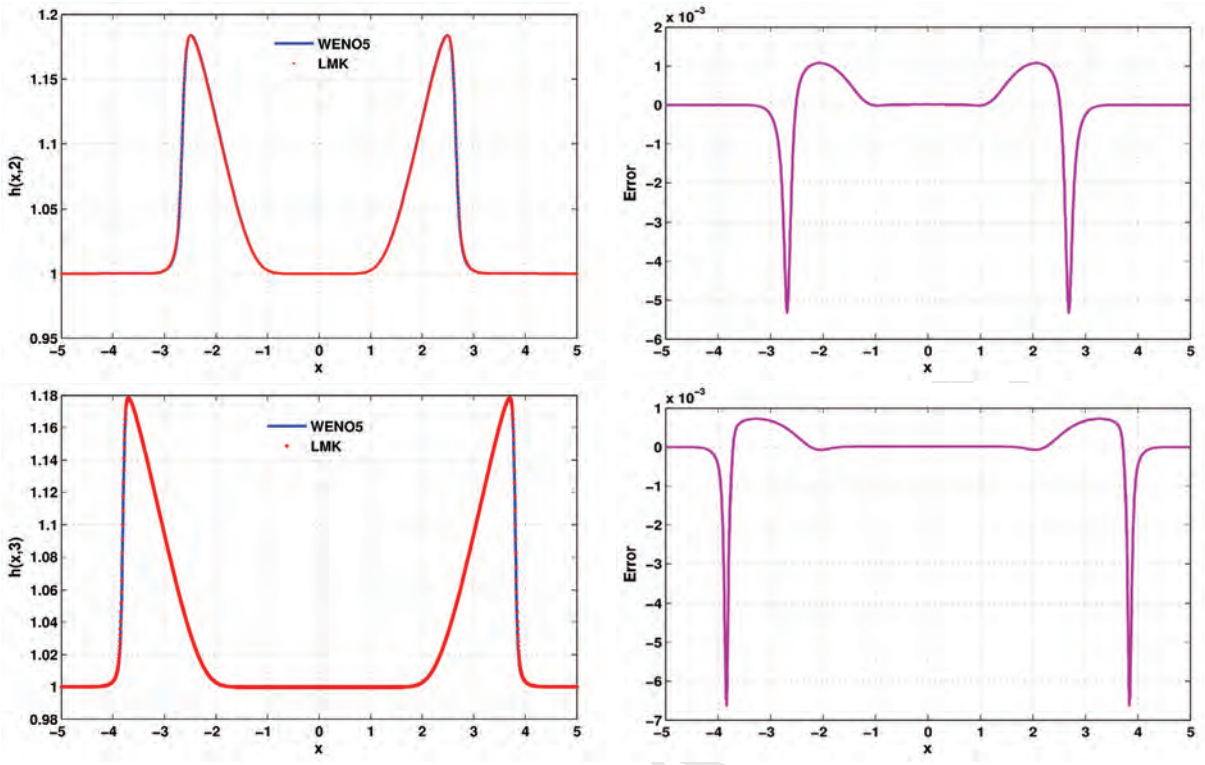

Figure 7: Graph of approximation solutions with $(m = 10, n_s = 11)$ based on the LMK for Test problem 2.

Table 3: Errors obtained for Test problem 2

	$T = 2$		$T = 3$	
Number of nodes	RBF-FD	LMK	RBF-FD	LMK
2^7	7.0342×10^{-3}	1.3405×10^{-2}	1.6194×10^{-3}	7.7818×10^{-3}
2^{10}	8.2628×10^{-4}	1.1897×10^{-3}	1.4485×10^{-4}	5.0967×10^{-4}
2^{12}	8.2731×10^{-5}	1.3470×10^{-4}	1.0541×10^{-5}	3.2443×10^{-5}

and the achieved numerical results using LRBFs be the approximation solution. Then, we obtained the difference between these solutions and plotted an error graph in Figure 6.

Figure 7 presents the approximation solution using local collocation method based on shape functions of moving Kriging interpolation method with 2^{11} total number nodes and support radius $5 * dx$ at two final times $T = 2$ (up figures) and $T = 3$ (down figures). The error graph in Figure 7 is similar to Figure 6.

Figures 6 and 7 display the evolution of a hump of water. Similar to the acoustics equations [66], the hump gives rise to two waves, one moving in each direction. As is said in [66], when the height of the hump was very small compared to the background depth $h0 = 1$, then these would propagate with their shape essentially unchanged, at the characteristic speeds [66]. In Figures 6 and 7 the variation in depth is sufficiently large that the nonlinearity plays a clear role. The front of the wave steepens through a compression wave into a shock, while the back spreads out as a

rarefaction wave [66].

5.3 Test problem 3 (The shallow water equation with friction term).

We consider the shallow water equation with friction term as follows [11, 37]

$$\begin{cases} \dfrac{\partial h}{\partial t} + \dfrac{\partial (uh)}{\partial x} = 0, \\ \\ \dfrac{\partial (uh)}{\partial t} + \dfrac{\partial (hu^2 + 0.5gh^2)}{\partial x} = -ghB_x(x) - n^2 \dfrac{\sqrt{(uh)^2}}{h^\gamma}(uh), \end{cases} \tag{5.9}$$

in which

$$\begin{aligned} B(x) &= \sin^2(\pi x), \\ h(x,0) &= 5 + \exp(\cos(2\pi x)), \\ hu(x,0) &= \sin(\cos(2\pi x)). \end{aligned}$$

The current example is devoted to the analysis of the accuracy. To test the ability of the proposed

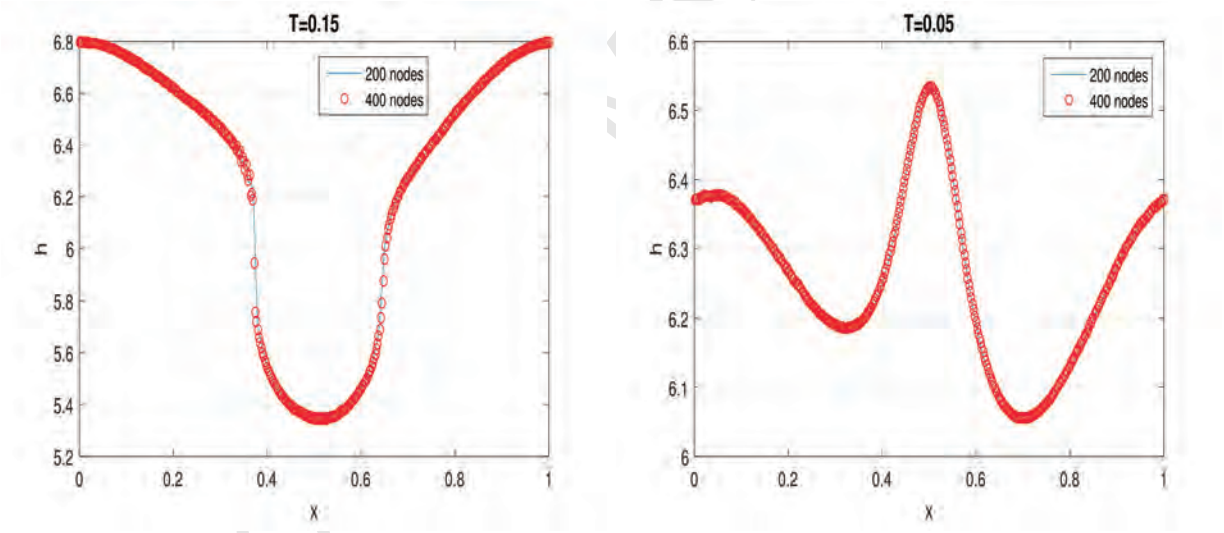

Figure 8: Graphs of approximation solution with $(m = 10, n_s = 17)$ using the LRBFs method for Test problem 3.

technique, we use the experimentally validated Manning-Chezy formulation [44] for the friction term [11, 37]

$$\mathcal{F}(U) = \begin{pmatrix} 0 \\ n^2 \dfrac{\sqrt{(uh)^2}}{h^\gamma}(uh) \end{pmatrix}. \tag{5.10}$$

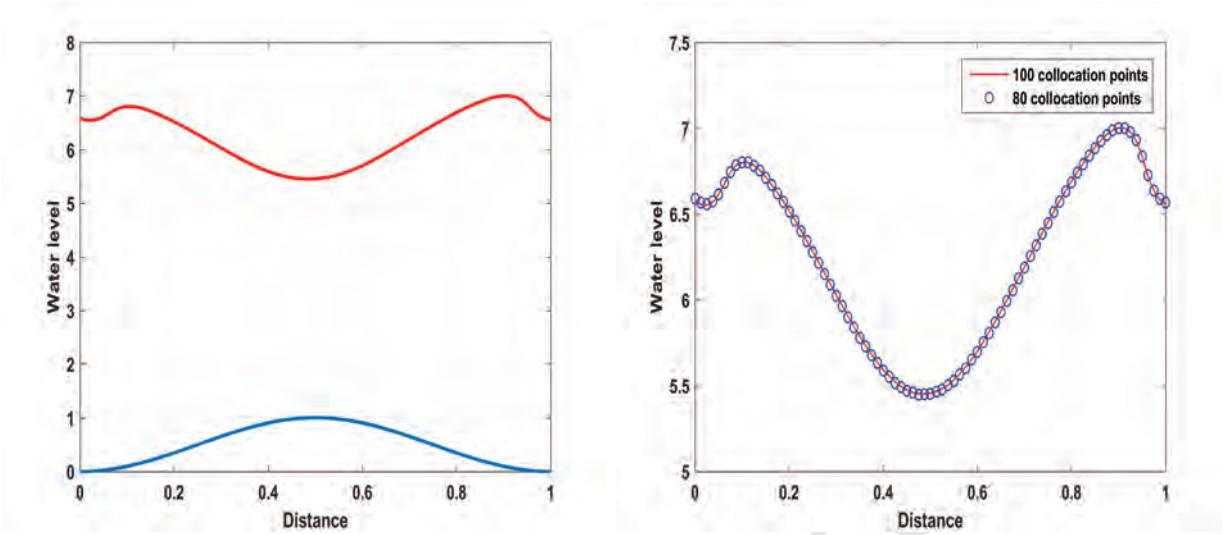

Figure 9: Graphs of approximation solution with $(m = 10, n_s = 17)$ using the LRBFs method for Test problem 3.

As is said in [11], in some special cases, it may be important to ensure that the flow may be arrested by large enough friction force but not be reversed by them. In the current example, we consider

Table 4: The used CPU time(s) for Test problem 3

		Computational Time	
Number of nodes	Number of POD bases	RBF-FD	POD
128	12	43	6.7
256	14	78	9.2
512	18	113	11.3
1024	24	265	13.7
2048	30	355	16.5

Table 5: Errors obtained for Test problem 3

	$T = 0.05$		$T = 0.15$	
Number of nodes	RBF-FD	LMK	RBF-FD	LMK
10000	7.1961×10^{-2}	2.3785×10^{-1}	4.3645×10^{-2}	8.7839×10^{-1}
20000	4.5347×10^{-2}	6.4472×10^{-2}	5.7038×10^{-3}	5.8001×10^{-2}
40000	3.1366×10^{-3}	1.0249×10^{-2}	1.3997×10^{-3}	1.3146×10^{-2}

$\gamma = 10/3$. Figure 8 illustrates the graphs of approximation solution using different values of nodes i.e. 400 and 200 collocation nodes and also for $n = 0.035$ using the LRBFs method for Test problem 3. Table 4 shows the used CPU time(s) for Test problem 3. Similar to Test problem 2, we consider the obtained numerical results by WENO method [67] as an exact solution and then we compare

them with the numerical schemes in the current paper i.e. RBF-FD and LMK methods and also report the errors in Table 5 for Test problem 3.

5.4 Test problem 4 (Model of water in the middle of a bathtub or a smooth surface wave propagation).

We consider the two-dimensional shallow water equation as [39]

$$\begin{cases} \dfrac{\partial h}{\partial t}+\dfrac{\partial\left(uh\right)}{\partial x}+\dfrac{\partial\left(vh\right)}{\partial x}=0, \\ \dfrac{\partial\left(uh\right)}{\partial t}+\dfrac{\partial\left(u^{2}h+0.5gh^{2}\right)}{\partial x}+\dfrac{\partial\left(uvh\right)}{\partial y}=0, \\ \dfrac{\partial\left(vh\right)}{\partial t}+\dfrac{\partial\left(v^{2}h+0.5gh^{2}\right)}{\partial y}+\dfrac{\partial\left(uvh\right)}{\partial x}=0, \end{cases} \tag{5.11}$$

with the following initial conditions

$$\begin{cases} h(x,y,0)=1+\exp\left(-\frac{\left(x^{2}+y^{2}\right)}{0.001}\right), \\ (uh)(x,y,0)=0, \\ (vh)(x,y,0)=0, \end{cases}$$

and reflective boundary conditions. As is mentioned in [80] in the study of surface wave propagation, the ice cover is conventionally modeled by a thin elastic plate. The appeared waves are referred to as flexural gravity ones on the assumption that the particle motion in them is governed by gravity, particle inertia, and surface tension acting upon water from the deformed ice cover. The main approximations of this model are the following: the wave's amplitude is small compared to its length; the plate thickness is small related to its curvature radius; and the ice elasticity greatly exceeds its viscosity, relaxation, and plasticity. The model is valid for waves of lengths greater than 100 m and amplitudes less than a few meters [80].

We solved the current example using the present methods. Figure 10 shows a schematic for the initial condition for this problem. The full model is solved using 30000 collocation points in the computational region and 90 points in each subdomain and also $dt = 10^{-4}$. Figure 14 demonstrates graphs of approximation solution and their contours for component h at different values of final times for Test problem 4. Figure 15 presents graphs of approximation solution and their contours with $(m = 20, n_s = 21)$ for component h on circular domain at different values of final times for Test problem 4. Figure 11 demonstrates the singular values of the coefficient matrix of local RBF-FD scheme and this figure shows the first singular value has the largest magnitude and also the remainder singular values are decreasing with a fast speed. Also, following descriptions can be found with more details in [126]. By calculating the singular values, we can see $\lambda_1 0 \leq 6.7411 \times 10^{-10}$ for 800 collocation node. In other hand, from Eq. (4.5), we have $I(1) = 0.99742$ and $I(7) = 0.999998$. Thus, we can say if $\lambda_{i+1} \leq 6.7411 \times 10^{-10}$, i POD bases will be suitable as the number of the

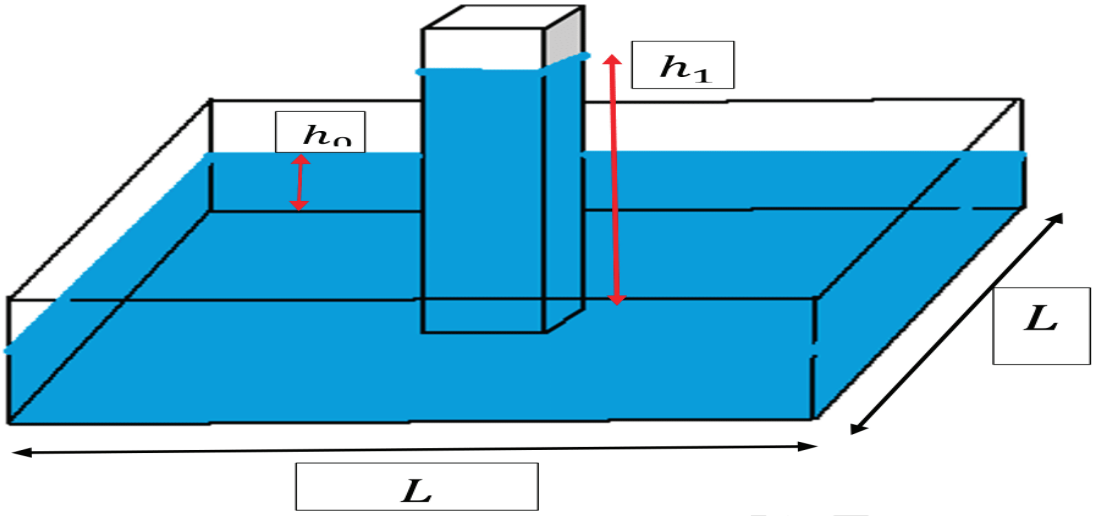

Figure 10: A schematic for the initial condition for Test problem 4

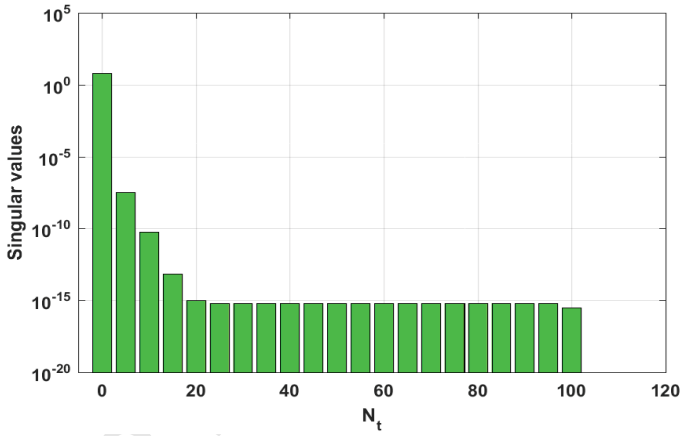

Figure 11: Distribution of singular value for Test problem 4.

optimal POD basis. Then for Test problem 4, we take 20 POD basis for 800 nodes. Also, **RMSE** and **Corr** errors based on the POD-LRBF-FD methods with 100 POD basis for Test problem 4 are depicted in Figure 12. Figure 13 presents CPU time of the full system, POD reduced systems and (left panel) and singular values of the snapshots solutions h, u and v (right panel) for Test problem 4.

5.5 Test problem 5. (Simulation of a dam-break flow)

Removing a vertical barrier yields the dam-break flow. A dam-break flow is an uncontrolled release of water when a vertical barrier is removed suddenly and it is the simplest available model for many important phenomena [77]. The dam-break flow can be described for several phenomena for example as break-out floods, sheet flow events, and the formative stages of lahars or debris flows

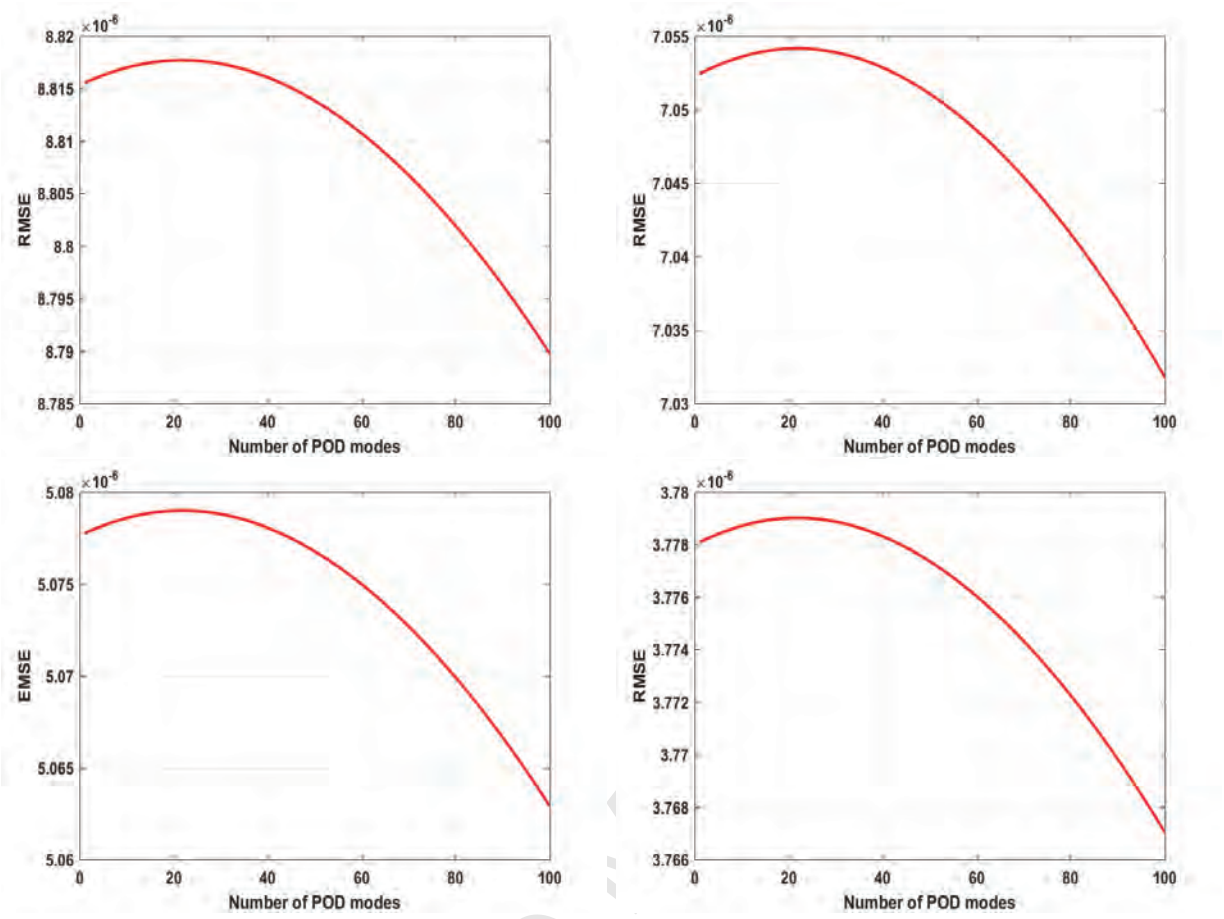

Figure 12: **RMSE** and **Corr** errors based on the POD-LRBF-FD methods with 100 POD basis for Test problem 4.

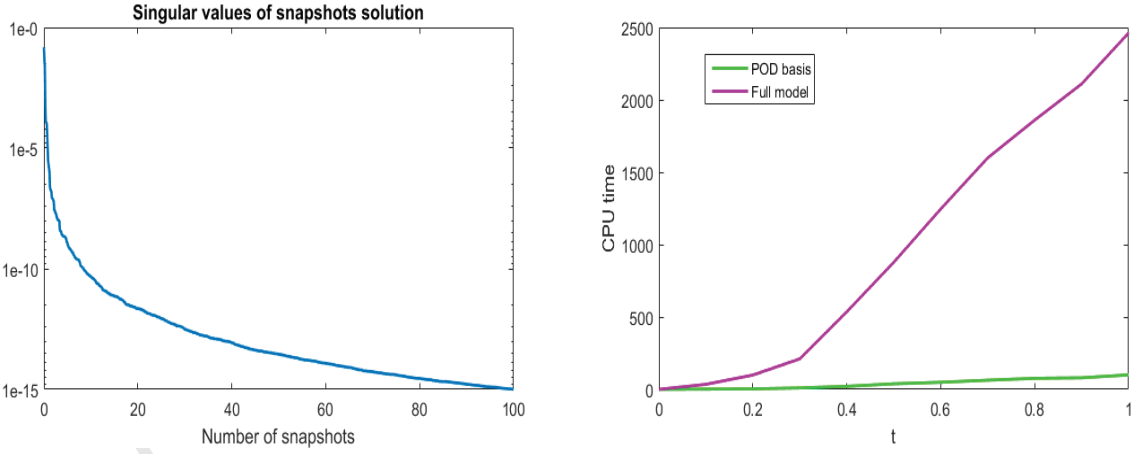

Figure 13: CPU time of the full system, POD reduced systems and (left panel) and singular values of the snapshots solutions h, u and v (right panel) for Test problem 4.

[77]. Thus, in the numerical results we considered many nodes in the computational domain. We

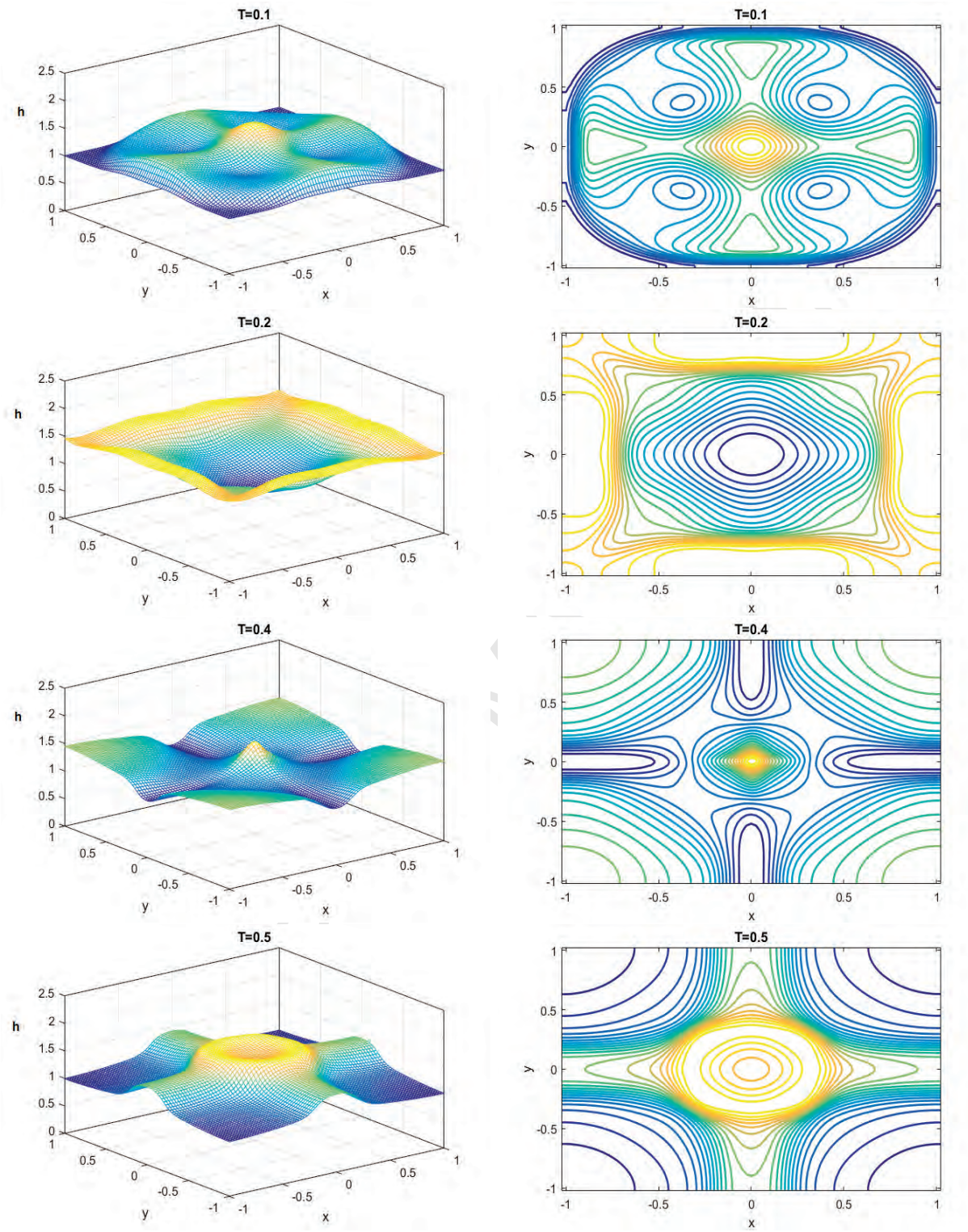

Figure 14: Graphs of approximation solution and their contours with $(m = 20, n_s = 21)$ for component h on rectangular domain at different values of final times for Test problem 4.

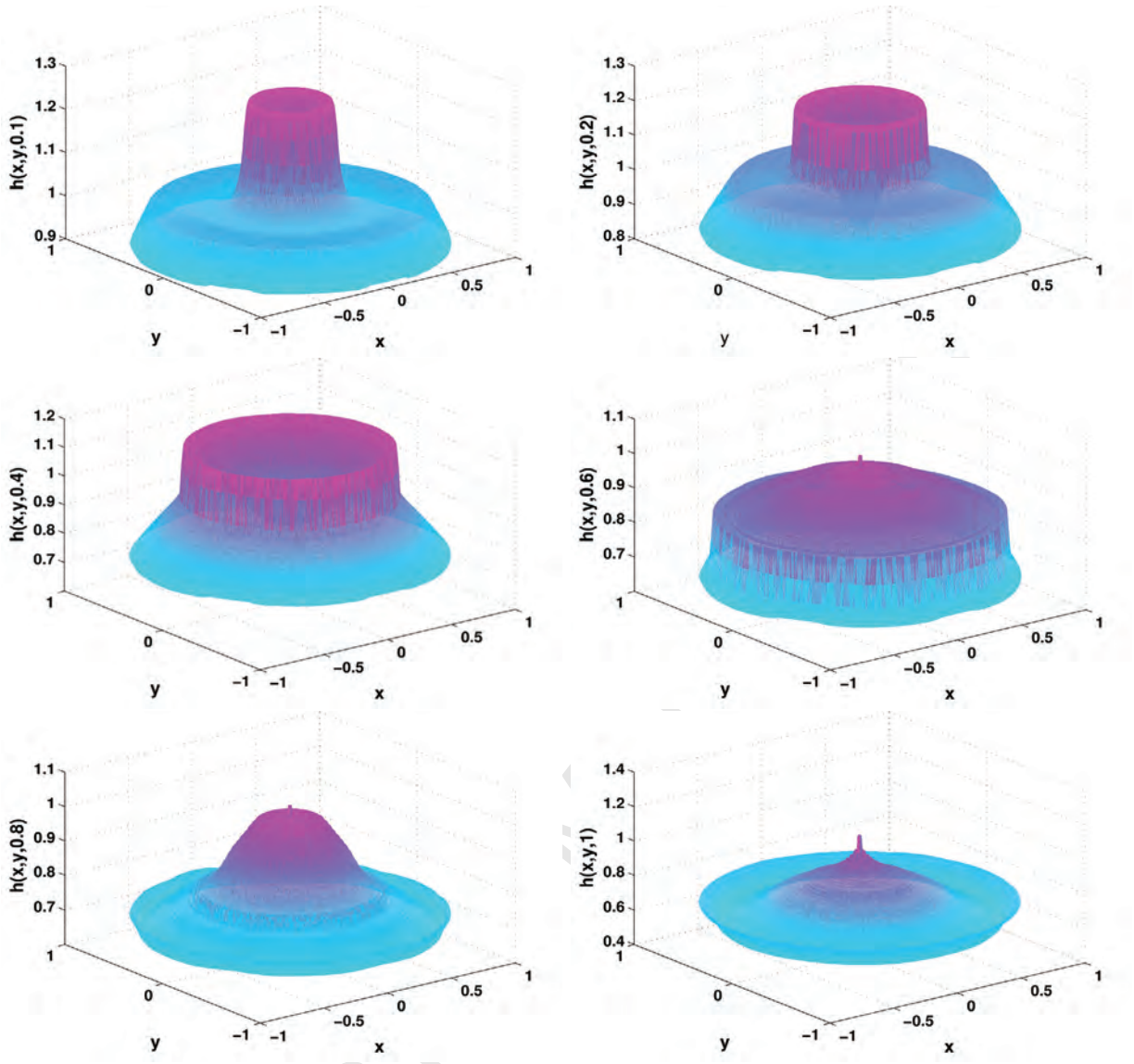

Figure 15: Graphs of approximation solution and their contours with ($m = 20, n_s = 21$) for component h on circular domain using LMK technique at different values of final times for Test problem 4.

consider model (2.41) with the following parameters [77]

$$\gamma = 0.001, \qquad f = 1.1 \times 10^{-4}, \qquad \theta = 7.5 \times 10^{-3}, \qquad \alpha = 0.35,$$

$$g = 9.8, \qquad c_D = 0.01, \qquad \varepsilon = 0.35, \qquad \rho = 1.5 \times 10^{3}, \qquad \eta = 0.01.$$

Figure 16 presents a schematic for the initial condition for Test problem 5. We solve the current test problem using the proposed technique. Figure 17 shows CPU time of the full system, POD reduced systems and (left panel) and singular values of the snapshots solutions w, u, v, ϕ and w_b (right panel) for Test problem 5. In the current paper, at first, we employ a simple example as the gate has width 100 m. Figure 18 shows the singular values of the coefficient matrix of local RBF-FD scheme and this figure shows the first singular value has the largest magnitude and also

the remainder singular values are decreasing with a fast speed. By calculating the singular values, we can see $\lambda_1 8 \leq 7.3746 \times 10^{-10}$ for 800 collocation node. In other hand, from Eq. (4.5), we have $I(1) = 0.99610$ and $I(7) = 0.99989$. Thus, we can say if $\lambda_{i+1} \leq 7.3746 \times 10^{-10}$, i POD bases will be suitable as the number of the optimal POD basis. Then for Test problem 5, we take 30 POD basis for 800 nodes. Also, **RMSE** and **Corr** errors based on the POD-LRBF-FD methods with 100 POD basis for Test problem 5 are depicted in Figure 19. Figure 20 illustrates the graph of approximation solutions related to components w based on the 30 POD basis for Test problem 5.

Now, for the second case, as is said in [77] an idealized model of the dam-break flow may show that the barrier at $x = 0.5$ and $0 \leq y \leq 1$ divides fluids of different depths 3 m and 1 m, until time $t = 0$ when a gate of width 0.5 m i.e. on $x = 0.2$ and $0.25 \leq y \leq 0.75$ in the barrier is removed instantaneously and fluid (depth 3 m) floods into the shallower region (depth 1 m). Thus, the computational domain for the dam-break flow problem is a square of area $1 \times 1\ m^2$, i.e., $\Omega = [0, 1] \times [0, 1]$, which holds water depths of 3 m on the sub-domain $[0, 0.2] \times [0, 1]$ and 1 m on the sub-domain $[0.2, 1] \times [0, 1]$. Graphs of approximation solutions with their contours with $(m = 30, n_s = 31)$ related to components w for Test problem 5 are presented in Figure 21.

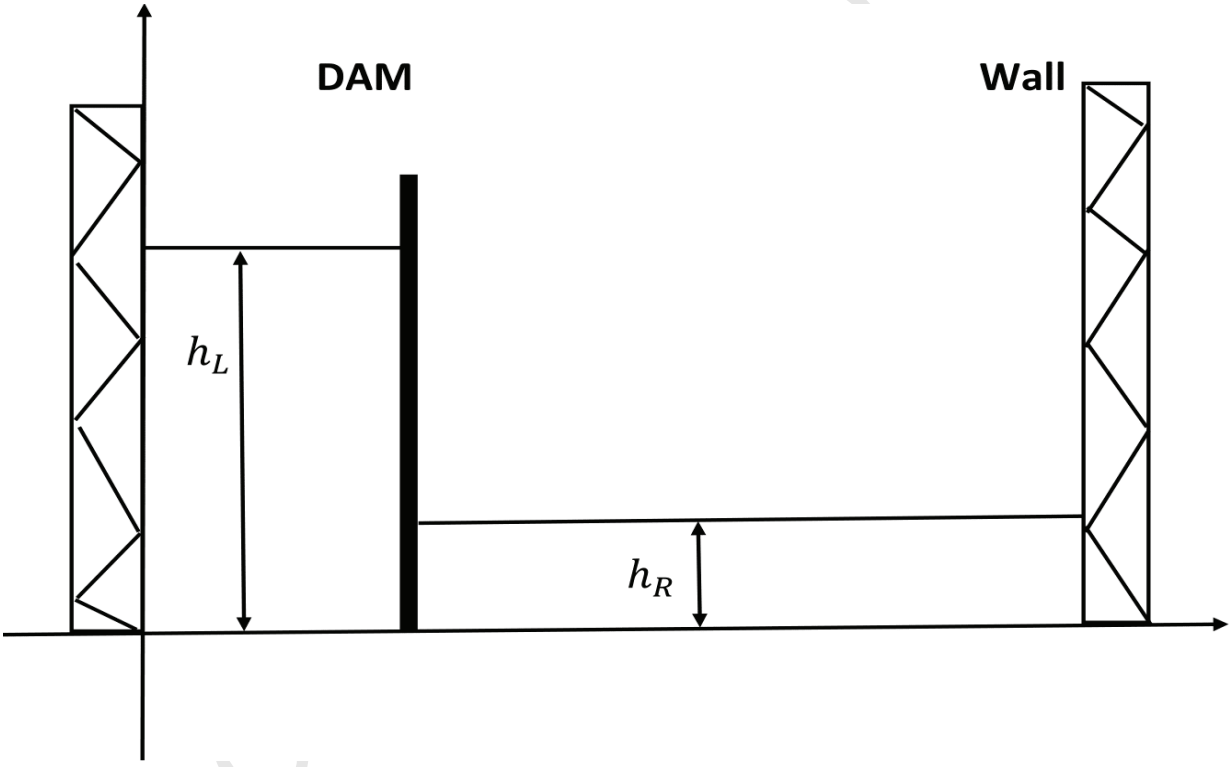

Figure 16: A schematic for the initial condition for Test problem 5.

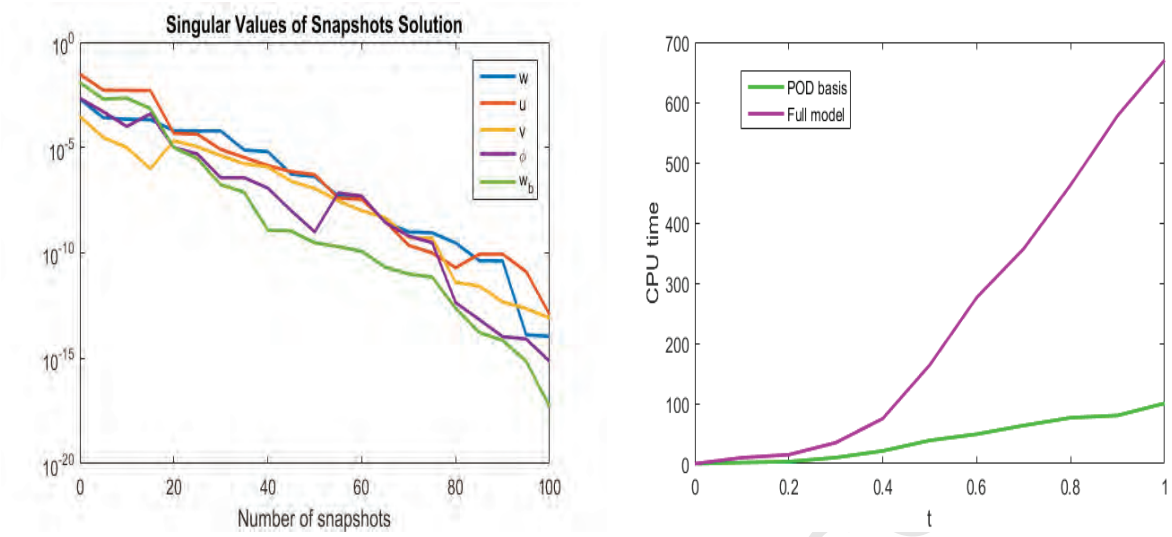

Figure 17: CPU time of the full system, POD reduced systems and (left panel) and singular values of the snapshots solutions w, u, v, ϕ and w_b (right panel) for Test problem 5.

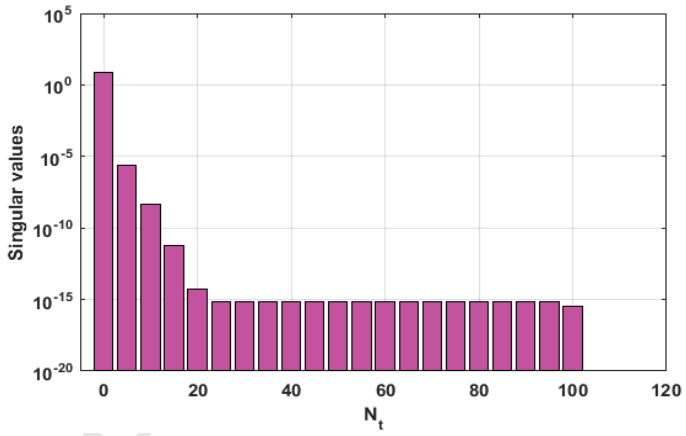

Figure 18: Distribution of singular value for Test problem 5.

5.6 Test problem 6 (Model of water in a bathtub with friction term).

We consider the shallow water equation with friction term as follows [39]

$$\begin{cases} \dfrac{\partial h}{\partial t} + \dfrac{\partial (uh)}{\partial x} + \dfrac{\partial (vh)}{\partial y} = 0, \\ \dfrac{\partial (uh)}{\partial t} + \dfrac{\partial (u^2 h + 0.5gh^2)}{\partial x} + \dfrac{\partial (uvh)}{\partial y} = -n^2 \dfrac{\sqrt{(uh)^2 + (vh)^2}}{h^\gamma}(uh), \\ \dfrac{\partial (vh)}{\partial t} + \dfrac{\partial (v^2 h + 0.5gh^2)}{\partial y} + \dfrac{\partial (uvh)}{\partial x} = -n^2 \dfrac{\sqrt{(uh)^2 + (vh)^2}}{h^\gamma}(vh), \end{cases} \tag{5.12}$$

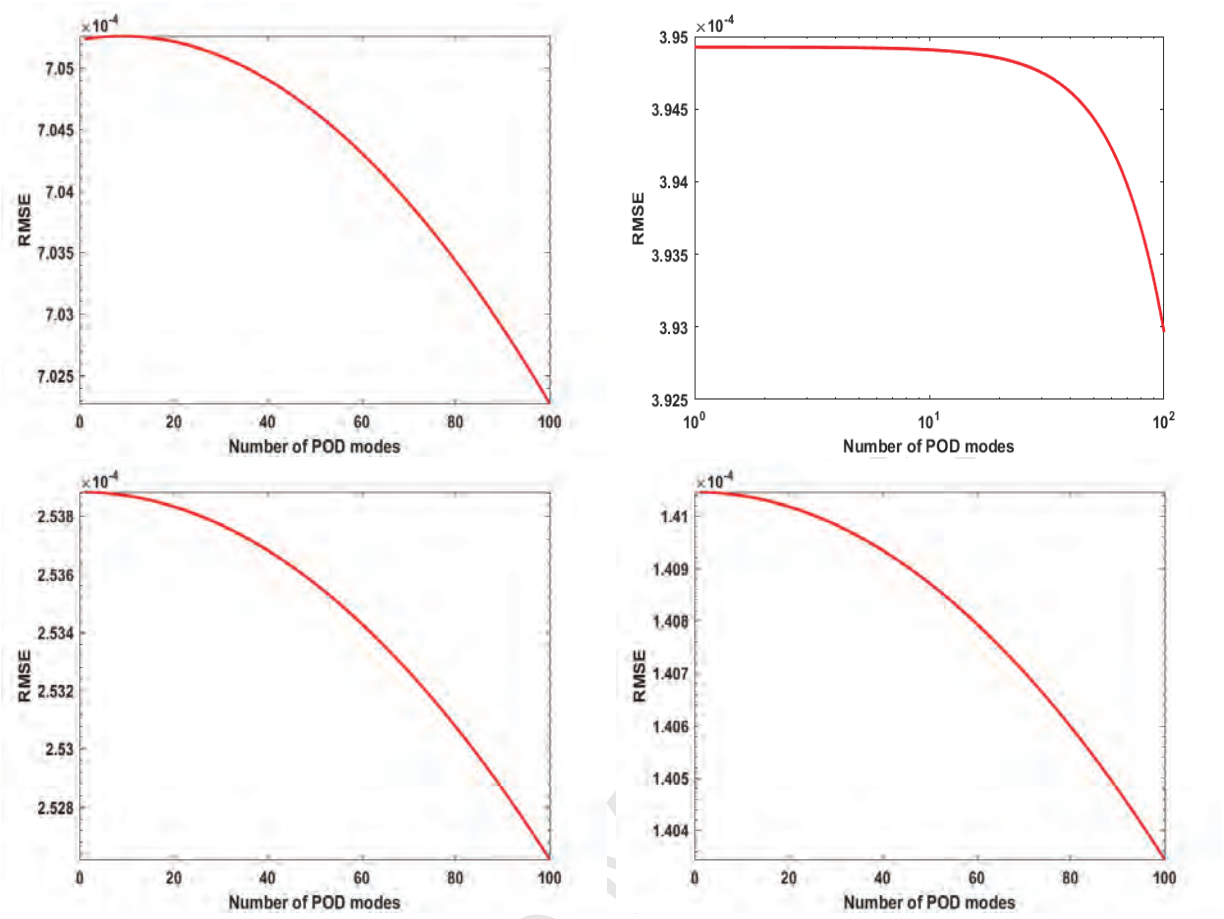

Figure 19: **RMSE** and **Corr** errors based on the POD-LRBF-FD methods with 100 POD basis for Test problem 5.

with the following initial conditions

$$\begin{cases} h(x,y,0) = \begin{cases} 1.0, & 0 \le y \le 10, \quad 110 \le x \le 120, \\ 0.1, & \text{o.w.} \end{cases} \\ uh(x,y,0) = 0, \\ vh(x,y,0) = 0, \end{cases}$$

and reflective boundary conditions. Figure 23 shows the singular values of the coefficient matrix of local RBF-FD scheme and this figure shows the first singular value has the largest magnitude and also the remainder singular values are decreasing with a fast speed. By calculating the singular values, we can see $\lambda_2 0 \le 4.3385 \times 10^{-10}$ for 800 collocation node. In other hand, from Eq. (4.5), we have $I(1) = 0.99042$ and $I(7) = 0.99998$. Thus, we can say if $\lambda_{i+1} \le 4.3385 \times 10^{-10}$, i POD bases will be suitable as the number of the optimal POD basis. Then for Test problem 6, we take 40 POD basis for 800 nodes. Also, **RMSE** and **Corr** errors based on the POD-LRBF-FD methods with 100 POD basis for Test problem 6 are depicted in Figure 24. Figure 25 displays outputs of a

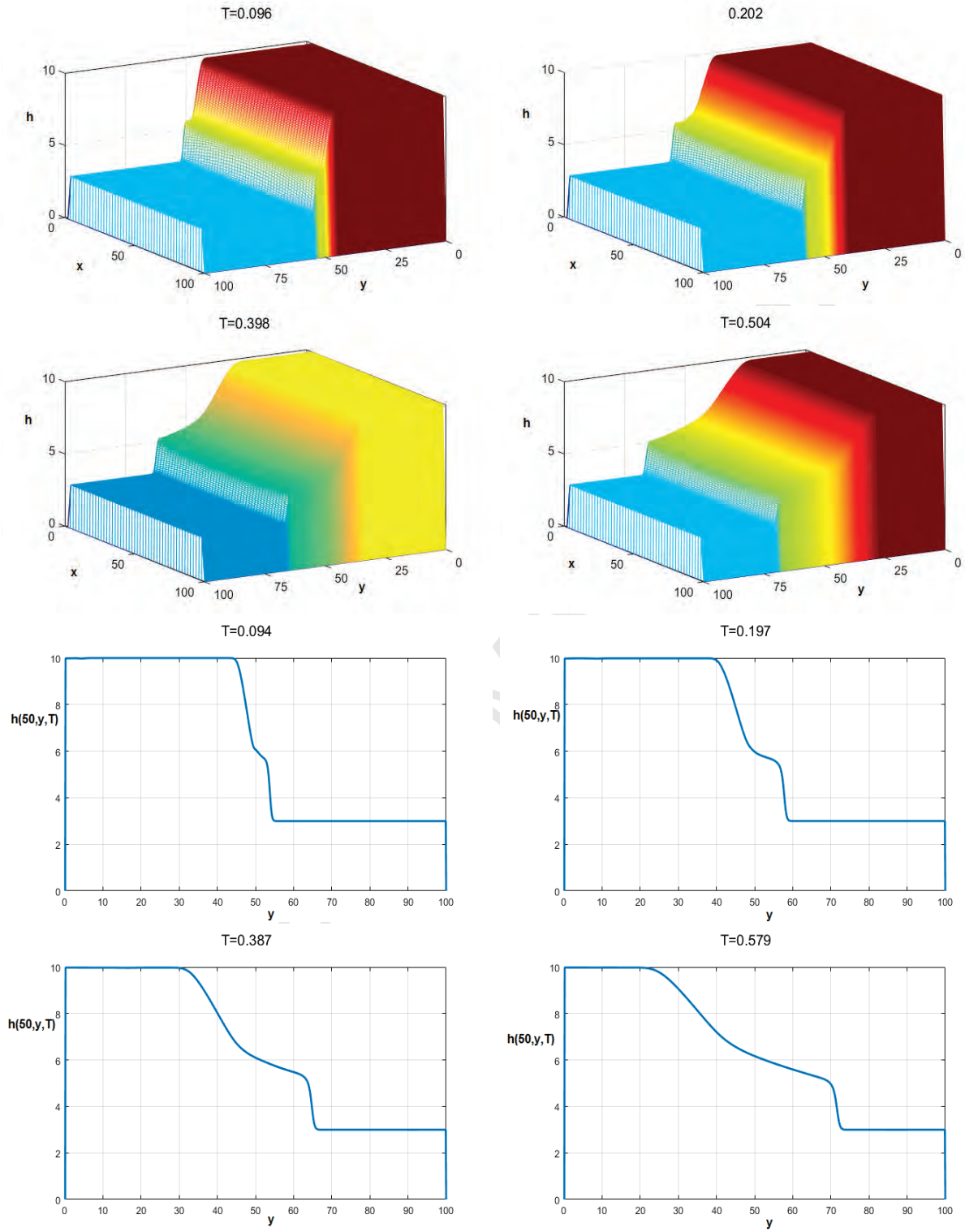

Figure 20: Graph of approximation solutions with $(m = 30, n_s = 31)$ related to components w for Test problem 5.

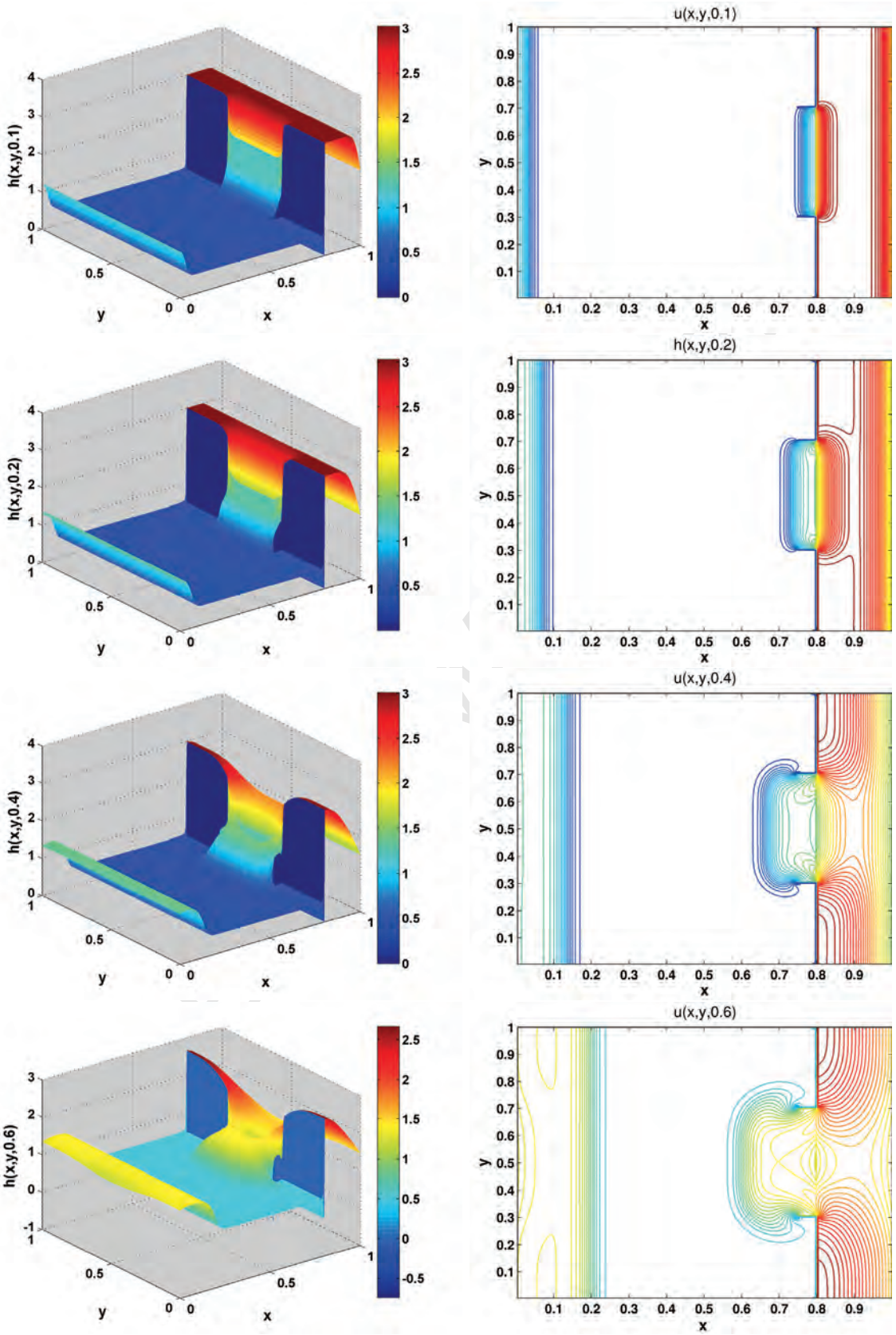

Figure 21: Graphs of approximation solutions with $(m = 30, n_s = 31)$ related to components w for Test problem 5.

shallow water equation for modelling of water in a bathtub. We solved the current example using the present method. In this problem $B(x, y) = 0$ and a friction term with $\gamma = 10/3$ is appeared in the model. Figure 22 depicts CPU time of the full system, POD reduced systems and (left panel) and singular values of the snapshots solutions h, u and v (right panel) for Test problem 6.

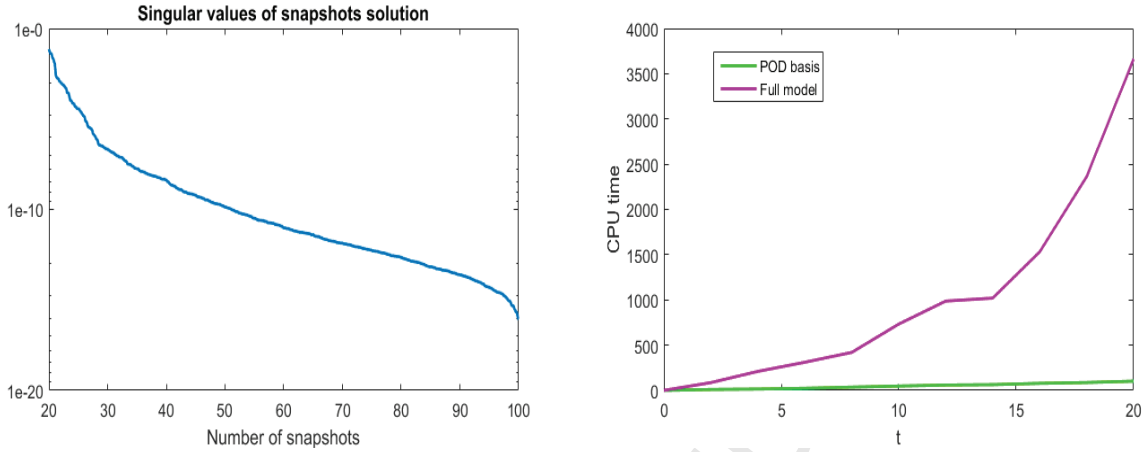

Figure 22: CPU time of the full system, POD reduced systems and (left panel) and singular values of the snapshots solutions h, u and v (right panel) for Test problem 6.

6 Conclusion

In many areas of of applied sciences, such as chemistry, physics, fluid mechanics and etc, we have to solve the advection and advection-diffusion-reaction equations. These equations are very important and sometimes finding their analytic solutions is so difficult. Thus, applying a useful numerical method for these equations is a topic of interest for researchers. The shallow water equation is an important equation in fluid mechanics for simulating the height and velocity of water. In this paper, we suggest a fast numerical method using the proper orthogonal decomposition approach for solving the mentioned equations. The local collocation technique is presented to obtain a numerical algorithm for solving equations which arise in water sciences. The method presented here is based on the RBF approximation and finite difference approach that produces the RBF-FD technique. Also, in the current paper, we combined the RBF-FD method with the proper orthogonal decomposition approach to reduce the CPU time. The technique developed is applied on six test problems and simulation results confirm that the new procedure is appropriate for finding the approximate solutions of our models.

Acknowledgment:

The authors are grateful to the reviewers for carefully reading this paper and for their comments and suggestions which really have improved the paper.

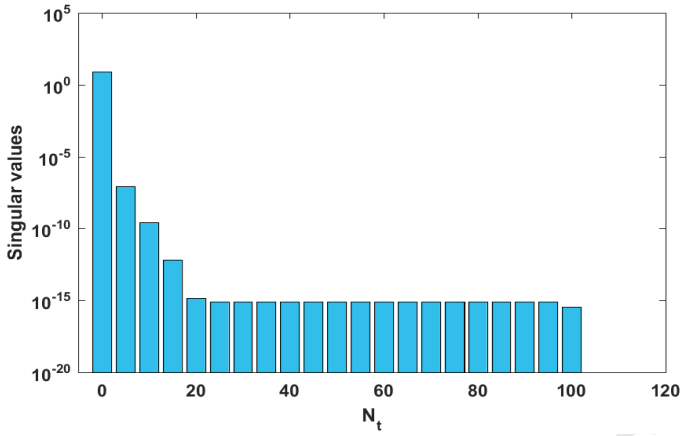

Figure 23: Distribution of singular value for Test problem 6.

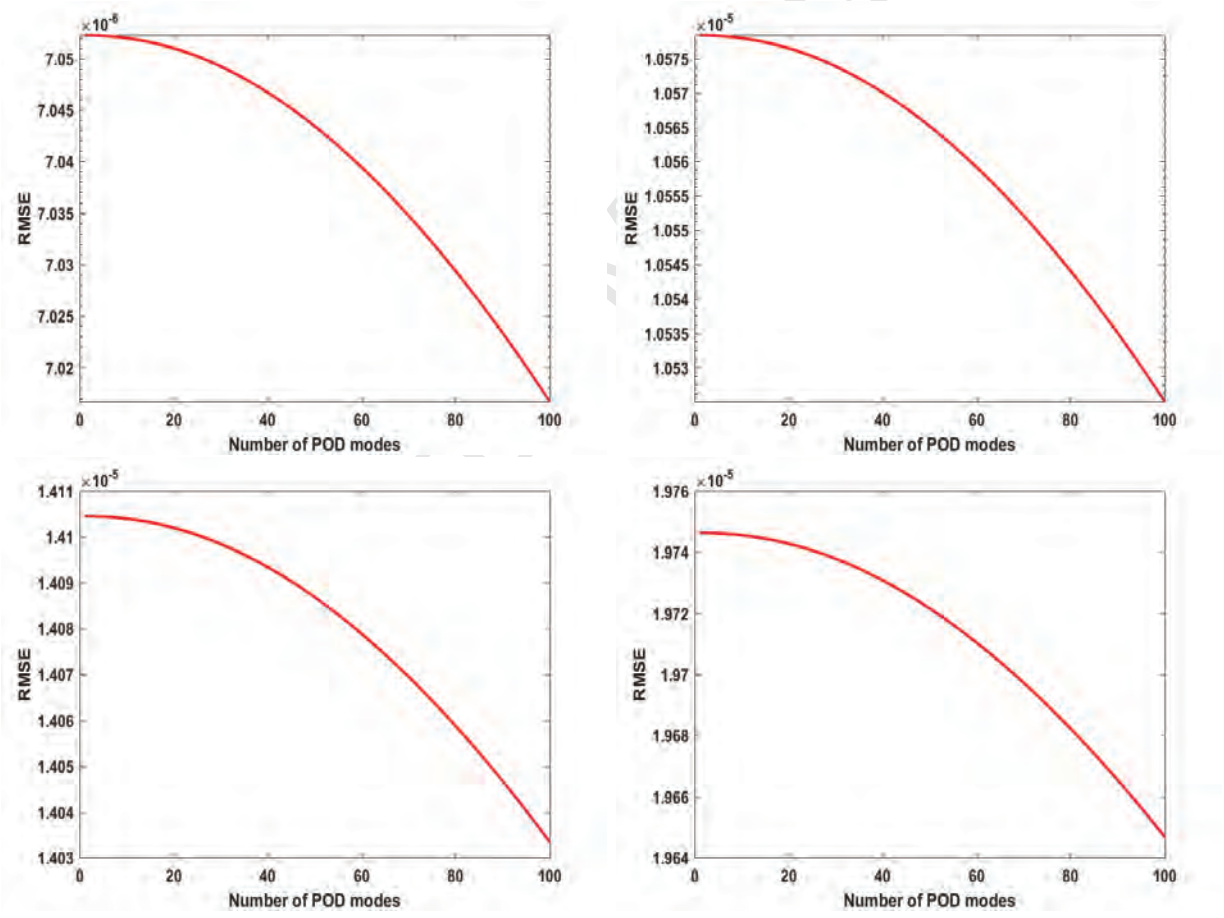

Figure 24: **RMSE** and **Corr** errors based on the POD-LRBF-FD methods with 100 POD basis for Test problem 6.

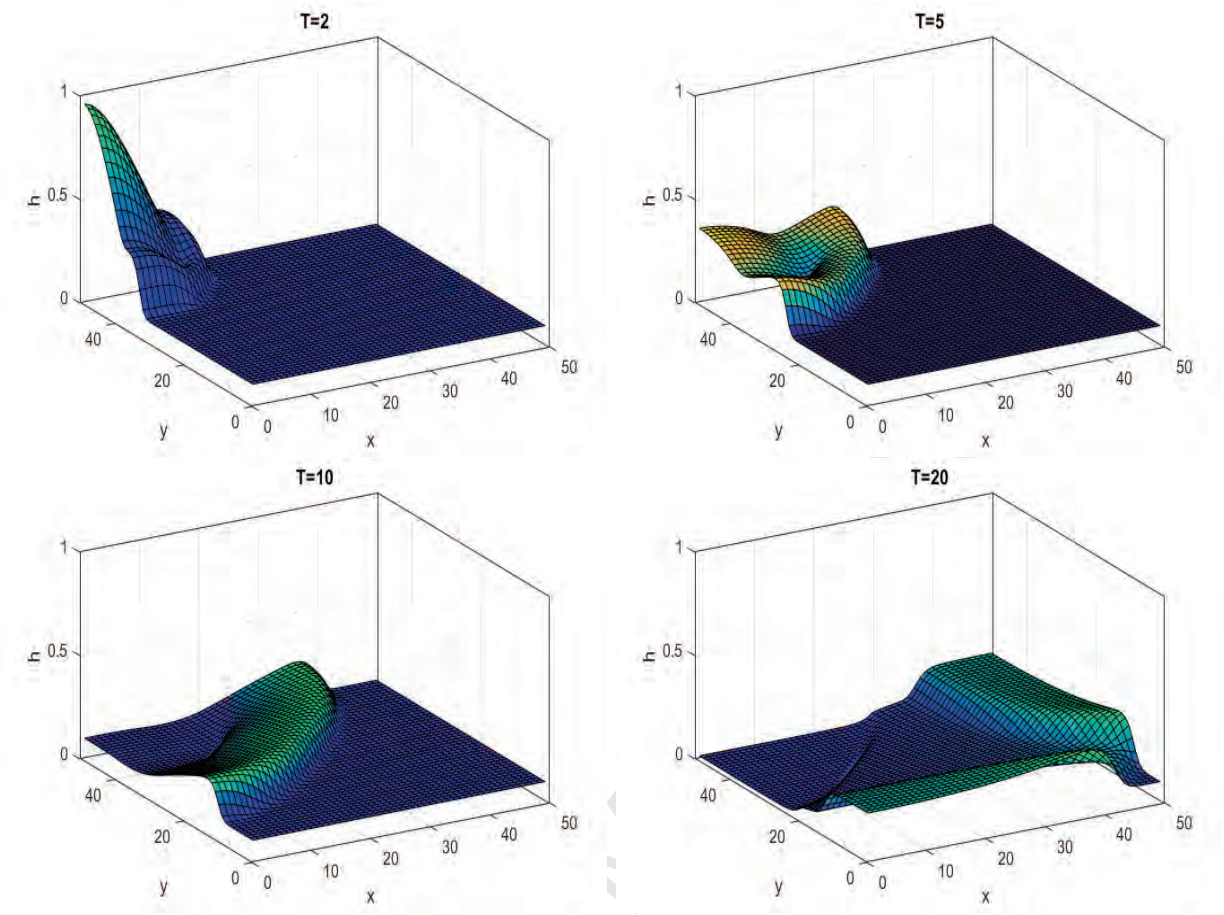

Figure 25: Graphs of approximation solution and their contours with ($m = 40, n_s = 31$) for component u using LMK technique at different values of final time for Test problem 6.

References

[1] F. Alcrudoa, F. Benkhaldoun, Exact solutions to the Riemann problem of the shallow water equations with a bottom step, Computers & Fluids 30 (2001) 643-671.

[2] F. Benkhaldoun, A. Halassi, D. Ouazar, M. Seaid, Ahmed Taik, A stabilized meshless method for time-dependent convection-dominated flow problems, Math. Comput. Simul. 137 (2017) 159-176.

[3] F. Benkhaldoun, M. Seaïd, A simple finite volume method for the shallow water equations, J. Comput. Appl. Math. 234 (2010) 58-72.

[4] F. Benkhaldoun, A. Halassi, D. Ouazar, M. Seaid, A. Taik, Slope limiters for radial basis functions applied to conservation laws with discontinuous flux function, Engin. Anal. Bound. Elem. 66 (2016) 49-65.

[5] F. Benkhaldoun, S. Sari, M. Seaid, Projection finite volume method for shallow water flows, Math. Comput. Simul. 118 (2015) 87-101.

[6] F. Benkhaldoun, I. Elmahi, A. Moumna, M. Seaid, A non-homogeneous Riemann solver for shallow water equations in porous media, Applicable Analysis, 95 (2016) 2181-2202.

[7] G. Berkooz, P. Holmes, J. L. Lumley, The proper orthogonal decomposition in the analysis of turbulent flows, Annual Review of Fluid Mechanics, 25.1 (1993) 539-575.

[8] A. Bermudez, M.E. Vazquez-Cendon, Upwind methods for hyperbolic conservation laws with source terms, Comput. & Fluids 23 (1994) 1049-1071.

[9] C. Berthon, F. Foucher, Efficient well balanced hydrostatic upwind schemes for shallow water equations, J. Comput. Phys. 231 (2012) 4993-5015.

[10] C. Berthon, P. LeFloch, R. Turpault, Late-time/stiff-relaxation asymptotic-preserving approximations of hyperbolic equations, Math. Comput. 82 (2013) 831-860.

[11] C. Berthon, F. Marche, R. Turpault, An efficient scheme on wet/dry transitions for shallow water equations with friction, Comput. Fluids 48 (2011) 192-201.

[12] C. Berthon, B. Boutin, R. Turpault, Shock profiles for the Shallow-water Exner models, Adv. Appl. Math. Mech., 7 (2015) 267-294.

[13] D. A. Bistrian, I. M. Navon, An improved algorithm for the shallow water equations model reduction: Dynamic Mode Decomposition vs POD, Int. J. Numer. Meth. Fluids, 78 (2015) 552-580.

[14] E. F. Bollig, N. Flyer, G. Erlebacher, Solution to PDEs using radial basis function finite differences (RBF-FD) on multiple GPUs, J. Comput. Phys., 231(21) (2012) 7133-7151.

[15] V. Bayona, M. Moscoso, M. Kindelan, Optimal constant shape parameter for multiquadric based RBF-FD method, J. Comput. Phy., 230 (2011) 7384-7399.

[16] V. Bayona, M. Moscoso, M. Kindelan, Optimal variable shape parameter for multiquadric based RBF-FD method, J. Comput. Phy., 231 (2012) 2466-2481.

[17] M. D. Buhmann, Radial Basis Functions: Theory and Implementations, Cambridge University Press, Cambridge, 2003.

[18] T. Q. Bui, C. Zhang, moving Kriging interpolation-based meshfree method for dynamic analysis of structures, Proc. Appl. Math. Mech. 11 (2011) 197-198.

[19] A. Canestrelli, M. Dumbser, Annunziato Siviglia, E. F. Toro, Well-balanced high-order centered schemes on unstructured meshes for shallow water equations with fixed and mobile bed, Adv. Water Resour, 33 (2010) 291-303.

[20] Y. Cao, J. Zhu, I. M. Navon, Z. Luo, A reduced-order approach to four-dimensional variational data assimilation using proper orthogonal decomposition, Int. J. Numer. Methods Fluids, 53 (2007) 1571-1583.

[21] Y. L. Chan, L. H. Shen, C. T. Wu, D. L. Young, A novel upwind-based local radial basis function differential quadrature method for convection-dominated flows, Computers & Fluids 89 (2014) 157-166.

[22] Y. L. Chan, L. H. Shen, C. T. Wu, D. L. Young, Interpolation techniques for scattered data by local radial basis function differential quadrature method, International Journal of Computational Methods, 10 (2013) Article number 1341011.

[23] S. Chaturantabut, Dimension Reduction for Unsteady Nonlinear Partial Differential Equations via Empirical Interpolation Methods, ProQuest, 2009.

[24] S. Chaturantabut, D. C. Sorensen, Nonlinear model reduction via discrete empirical interpolation, SIAM Journal on Scientific Computing 32 (5) (2010) 2737–2764.

[25] S. Chaturantabut, D. C. Sorensen, A state space error estimate for POD-DEIM nonlinear model reduction, SIAM J. Numer. Anal. 50 (1) (2012) 46–63.

[26] W. Chen, Z. J. Fu, C. S. Chen, Recent Advances in Radial Basis Function Collocation Methods, Springer Briefs in Applied Sciences and Technology, 2014.

[27] L. Chen, K. M. Liew, A local Petrov-Galerkin approach with moving Kriging interpolation for solving transient heat conduction problems, Comput. Mech., 47 (2011) 455-467.

[28] A. H. D. Cheng, Multiquadric and its shape parameter–A numerical investigation of error estimate, condition number, and round–of–error by arbitrary precision computation, Eng. Anal. Bound. Elem. 36 (2012) 220–239.

[29] C. J. Cotter, J. Thuburn, A finite element exterior calculus framework for the rotating shallow water equations, J. Comput. Phys. 257 (2014) 1506-1526.

[30] S. M. Cox, P. C. Matthews, Exponential time differencing for stiff systems, J. Comput. Phys., 176 (2002) 430-455.

[31] L. Cozzolino, L. Cimorelli, C. Covelli, R. D. Morte, D. Pianese, The analytic solution of the shallow-water equations with partially open sluice-gates: The dam-break problem, Adv. Water Resour, 80 (2015) 90-102.

[32] B. D. Dai, J. Cheng, B. J. Zheng, Numerical solution of transient heat conduction problems using improved meshless local Petrov-Galerkin method, Appl. Math. Comput., 219 (2013) 10044-10052.

[33] B. D. Dai, J. Cheng, B. J. Zheng, A moving Kriging interpolation-based meshless local Petrov-Galerkin method for elastodynamic analysis, International Journal of Applied Mechanics, 5(1) (2013) 1350011-1350021.

[34] T. A. Driscoll, B. Fornberg, Interpolation in the limit of increasingly flat radial basis functions, Comput. Math. Appl., 43 (2002) 413-422.

[35] J. Du, I. M. Navon, J. L. Steward, A. K. Alekseev, Z. Luo, Reduced-order modeling based on POD of a parabolized Navier-Stokes equation model I: forward model, Int. J. Numer. Meth. Fluids, 69 (2012) 710-730.

[36] J. Du, I. M. Navon, J. Zhu, F. Fang, A. K. Alekseev, Reduced order modeling based on POD of a parabolized Navier-Stokes equations model II: Trust region POD 4D VAR data assimilation, Comput. Math. Appl. 65 (2013) 380-394.

[37] A. Duran, F. Marche, R. Turpault, C. Berthon, Asymptotic preserving scheme for the shallow water equations with source terms on unstructured meshes, J. Comput. Phys. 287 (2015) 184-206.

[38] A. Duran, F. Marche, Q. Liang, On the well-balanced numerical discretization of shallow water equations on unstructured meshes, J. Comput. Phys. 235 (2013) 565-586.

[39] M. Dumbser, V. Casulli, A staggered semi-implicit spectral discontinuous Galerkin scheme for the shallow water equations, Appl. Math. Comput., 219 (2013) 8057-8077.

[40] R. Everson, L. Sirovich, Karhunen-Loeve procedure for gappy data, Journal of the Optical Society of America A 12(8), (1995) 1657-1664.

[41] F. Fang, C. Pain, I. Navon, G. Gorman, M. Piggott, P. Allison, P. Farrell, A. Goddard, A POD reduced order unstructured mesh ocean modelling method for moderate Reynolds number flows, Ocean Modelling 28 (1) (2009) 127–136.

[42] G. E. Fasshauer, Meshfree Approximation Methods with MATLAB, USA, World Scientific, 2007.

[43] J. Felcman, L. Kadrnka, Adaptive finite volume approximation of the shallow water equations, Appl. Math. Comput. 219 (2012) 3354-3366.

[44] A. A. Flamant, Mecanique Appliques-Hydraulique, Baudry et Cie, 1891.

[45] N. Flyer, E. Lehto, S. Blaise, G. B. Wright, A. St-Cyr, A guide to RBF-generated finite differences for nonlinear transport: Shallow water simulations on a sphere, J. Comput. Phys. 231 (2012) 4078-4095.

[46] B. Fornberg, E. Lehto, Stabilization of RBF-generated finite difference methods for convective PDEs, J. Comput. Phys. 230 (2011) 2270-2285.

[47] B. Fornberg, E. Lehto, C. Powell, Stable calculation of Gaussian-based RBF-FD stencils, Comput. Math. Appl., 65 (2013) 627-637.

[48] R. A. Gingold, J. J. Monaghan, Smoothed particle hydrodynamics: theory and application to non-spherical stars. Mon. Not. R. Astron. Soc., 181 (1977) 375-389.

[49] F. Gallerano, G. Cannata, M. Tamburrino, Upwind WENO scheme for shallow water equations in contravariant formulation, Comput. Fluids, 62 (2012) 1-12.

[50] V. Giovangigli, B. Tran, Mathematical analysis of a Saint-Venant model with variable temperature, Math. Models Methods Appl. Sci., 20 (8), (2010) 1251-1297.

[51] P. Gonzalez-Rodriguez, V. Bayona, M. Moscoso, M. Kindelan, Laurent series based RBF-FD method to avoid ill-conditioning, Engin. Anal. Bound. Elem., 52 (2015) 24-31.

[52] L. Gu, Moving Kriging interpolation and element-free Galerkin method, Int. J. Numer. Meth. Engng., 56 (2003) 1-11.

[53] Y. T. Gu, Q. X. Wang, K.Y. Lam, A meshless local Kriging method for large deformation analyses, Comput. Methods Appl. Mech. Engin., 196 (2007) 1673-1684.

[54] R. L. Hardy, Multiquadric equations of topography and other irregular surfaces, J. Geophys. Res. **76** (1971) 1705-1915.

[55] Y. C. Hon, B. Šarler, D. F. Yun, Local radial basis function collocation method for solving thermo-driven fluid-flow problems with free surface, Eng. Anal. Bound. Elem., 57 (2015) 2-8.

[56] C. T. Hsu, K, C, Yeh, Iterative explicit simulation of 1D surges and dam-break flows, Int. J. Numer. Meth. Fluids, 38 (2002) 647-675.

[57] S.-ul-Islam, R. Vertnik, B. Šarler, Local radial basis function collocation method along with explicit time stepping for hyperbolic partial differential equations, Appl. Numer. Math., 67 (2013) 136-151.

[58] S.-ul-Islam, B. Šarler, R. Vertnik, G. Kosec, Radial basis function collocation method for the numerical solution of the two-dimensional transient nonlinear coupled Burgers' equations, Appl. Math. Model. 36 (2012) 1148-1160.

[59] A. Javed, K. Djijdeli, J. T. Xing, Shape adaptive RBF-FD implicit scheme for incompressible viscous Navier-Strokes equations, Comput. Fluids, 89 (2014) 38-52.

[60] T. Jiang, Y. T. Zhang, Krylov implicit integration factor WENO methods for semilinear and fully nonlinear advection-diffusion-reaction equations, J. Comput. Phys. 253 (2013) 368-388.

[61] E. J. Kansa, Multiquadrics A scattered data approximation scheme with applications to computational fluid-dynamics – I, Comput. Math. Appl. 19 (1990) 127-145.

[62] E. J. Kansa, Multiquadrics A scattered data approximation scheme with applications to computational fluid dynamics - II, Comput. Math. Appl., 19 (1990) 147-161.

[63] K. K. Katta, R. D. Nair, V. Kumar, High-order finite volume shallow water model on the cubed-sphere: 1D reconstruction scheme, Appl. Math. Comput. 266 (2015) 316-327.

[64] G. Kerschen, J. Golinval, A. F. Vakakis, L. A. Bergman, The method of proper orthogonal decomposition for dynamical characterization and order reduction of mechanical systems: an overview, Nonlinear Dynamics, 41, no. 1-3 (2005) 147-169.

[65] K. Y. Lam, Q. X. Wang, H. Li, A novel meshless approach – Local Kriging (LoKriging) method with two-dimensional structural analysis, Comput. Mech. 33 (2004) 235-244.

[66] R. J. LeVeque, Finite Volume Methods for Hyperbolic Problems, Cambridge Texts in Applied Mathematics, Cambridge University Press, 2002.

[67] G. Li, V. Caleffi, J. Gao, High-order well-balanced central WENO scheme for pre-balanced shallow water equations, Comput. Fluids, 99 (2014) 182-189.

[68] X. Li, Error estimates for the moving least-square approximation and the element-free Galerkin method in n-dimensional spaces, Appl. Numer. Math., 99 (2016) 77-97.

[69] X. Li, Meshless Galerkin algorithms for boundary integral equations with moving least square approximations, Appl. Numer. Math., 61(12) (2011) 1237-1256.

[70] X. Li, J. Zhu, A Galerkin boundary node method and its convergence analysis, J. Comput. Appl. Math., 230(1) (2009) 314-328.

[71] Z. Lin, D. Xiao, F. Fang, C. C. Pain, I. M. Navon, Non-intrusive reduced order modelling with least squares fitting on a sparse grid, Intern. J. Numer. Methods Fluids, 83 (2017) 291–306.

[72] X. G. Li, B. D. Dai, L. H. Wang, A moving Kriging interpolation-based boundary node method for two-dimensional potential problems, Chin. Phys. B, 19(12) (2010) 120202-120207.

[73] B. Liu, An error analysis of a finite element method for a system of nonlinear advection-diffusion-reaction equations, Appl. Numer. Math. 59 (2009) 1947-1959.

[74] W. Liu, J. Huang, X. Long, Coupled nonlinear advection-diffusion-reaction system for prevention of groundwater contamination by modified upwind finite volume element method, Comput. Math. Appl. 69 (2015) 477-493.

[75] G. R. Liu, Y. T. Gu, An Introduction to Meshfree Methods and Their Programming, Springer Dordrecht, Berlin, Heidelberg, New York, 2005.

[76] L. Lucy, A numerical approach to the testing of fusion process, Astronomical J. 82 (1977) 1013-1024.

[77] Z. D. Luo, J. Gao, Z. Xie, Reduced-order finite difference extrapolation model based on proper orthogonal decomposition for two-dimensional shallow water equations including sediment concentration, J. Math. Anal. Appl., 429 (2015) 901-923.

[78] Z. D. Luo, J. Chen, I. M. Navon, X. Yang, Mixed finite element formulation and error estimate based on proper orthogonal decomposition for the nonstationary Navier-Stokes equations, SIAM J. Numer. Anal., 47 (2008) 1-19.

[79] Z. D. Luo, J. Chen, J. Zhu, R. Wang, I. M. Navon, An optimizing reduced order FDS for the tropical Pacific Ocean reduced gravity model, Int. J. Numer. Methods Fluids, 55 (2007) 143-161.

[80] A. V. Marchenko, K. I. Voliak, Surface wave propagation in shallow water beneath an inhomogeneous ice cover, Journal of Physical Oceanography 27 (1997) 1602-1613.

[81] K. Mramor, R. Vertnik, B. Šarler, Simulation of laminar backward facing step flow under magnetic field with explicit local radial basis function collocation method, Eng. Anal. Bound. Elem., 49 (2014) 37-47.

[82] A. Navas-Montilla, J. Murillo, Energy balanced numerical schemes with very high order, The augmented Roe flux ADER scheme, Application to the shallow water equations, J. Comput. Phys. 290 (2015) 188-218.

[83] S. Noelle, Y. Xing, C. W. Shu, High-order well-balanced finite volume WENO schemes for shallow water equation with moving water, J. Comput. Phy. 226 (2007) 29-58.

[84] S. Ravindran, Reduced-order adaptive controllers for fluid flows using POD, Journal of Scientific Computing 15 (4) (2000) 457–478.

[85] S. S. Ravindran, A reduced-order approach for optimal control of fluids using proper orthogonal decomposition, International Journal for Numerical Methods in Fluids 34 (5) (2000) 425–448.

[86] S. Rippa, An algorithm for selecting a good value for the parameter c in radial basis function interpolation, Adv. Comput. Math. 11 (1999) 193-210.

[87] S. A. Sarra, A local radial basis function method for advection-diffusion-reaction equations on complexly shaped domains, Appl. Math. Comput., 218 (2012) 9853-9865.

[88] S. A. Sarra, Adaptive radial basis function methods for time dependent partial differential equations, Appl. Numer. Math. 54 (2005) 79-94.

[89] S. A. Sarra, A linear system-free Gaussian RBF method for the Gross-Pitaevskii equation on unbounded domains, Numer. Methods Partial Differential Eq., 28 (2012) 389-401.

[90] A. Shokri, M. Dehghan, Meshless method using radial basis functions for the numerical solution of two–dimensional complex Ginzburg–Landau equation, Computer Modeling in Engineering and Science, CMES, **34** (2012) 333–358 .

[91] C. W. Shu, H. Ding, K.S. Yeo, Local radial basis function–based differential quadrature method and its application to solve two-dimensional incompressible Navier-Stokes equations, Comput. Methods Appl. Mech. Eng., 192 (2003) 941-954.

[92] C. W. Shu, H. Ding, N. Zhao, Numerical comparison of least square-based finite-difference (LSFD) and radial basis function-based finite-difference (RBF-FD) methods, Comput. Math. Appl., 51 (2006) 1297-1310.

[93] C. W. Shu, H. Ding, N. Zhao, Numerical comparison of least square–based finite–difference (LSFD) and radial basis function–based finite–difference (RBFFD) methods, Comput. Math. Appl. 51 (8), (2006) 1297–1310.

[94] C. W. Shu, H. Ding, H. Q. Chen, T. G. Wang, An upwind local RBF–DQ method for simulation of inviscid compressible flows, Comput. Methods Appl. Mech. Engrg. 194 (18), (2005) 2001–2017.

[95] C. P. Sun, D. L. Young, L. H. Shen, T. F. Chen, C. C. Hsian, Application of localized meshless methods to 2D shallow water equation problems, Eng. Anal. Bound. Elem., 37 (2013) 1339-1350.

[96] R. Ştefănescu, I. M. Navon, POD/DEIM nonlinear model order reduction of an ADI implicit shallow water equations model, Journal of Computational Physics 237 (2013) 95–114.

[97] R. Ştefănescu, A. Sandu, I. M. Navon, Comparison of POD reduced order strategies for the nonlinear 2D shallow water equations, International Journal for Numerical Methods in Fluids 76 (8) (2014) 497–521.

[98] A. I. Tolstykh, On using RBF-based differencing formulas for unstructured and mixed structured-unstructured grid calculations, in: Proceedings of the 16th IMACS World Congress, Lausanne, 2000.

[99] A. I. Tolstykh, D. A. Shirobokov, On using radial basis functions in a finite difference mode with applications to elasticity problems, Comput. Mech., 33 (2003) 68-79.

[100] M. Tavelli, M. Dumbser, A high order semi-implicit discontinuous Galerkin method for the two-dimensional shallow water equations on staggered unstructured meshes, Appl. Math. Comput. 234 (2014) 623-644.

[101] C. J. Trahan, C. Dawson, Local time-stepping in Runge-Kutta discontinuous Galerkin finite element methods applied to the shallow-water equations, Comput. Methods Appl. Mech. Engin., 217-220 (2012) 139-152.

[102] C. B. Vreugdenhil, Numerical Methods for Shallow-Water Flow, Dordrecht ; Boston : Kluwer Academic Publishers, 1994.

[103] Y. Wang, I. M. Navon, X. Wang, Y. Cheng, 2D burgers equation with large Reynolds number using POD/DEIM and calibration, International Journal for Numerical Methods in Fluids, 82 (2016) 909-931 .

[104] A. M. Wazwaz, Partial Differential Equations and Solitary Waves Theory, Springer Science & Business Media, 2010.

[105] H. Wendland, Scattered Data Approximation, in: Cambridge Monograph on Applied and Computational Mathematics, Cambridge University Press, 2005.

[106] Y. Xing, Exactly well-balanced discontinuous Galerkin methods for the shallow water equations with moving water equilibrium, J. Comput. Phys. 257 (2014) 536-553.

[107] Y. Xing, C. W Shu, High order finite difference WENO schemes with the exact conservation property for the shallow water equations, J. Comput. Phy., 208 (2005) 206-227.

[108] Y. Xing, X. Zhang, C. W. Shu, Positivity-preserving high order well-balanced discontinuous Galerkin methods for the shallow water equations, Advances in Water Resources, 33 (2010) 1476-1493.

[109] Y. Xing, C. W Shu, High-order finite volume WENO schemes for the shallow water equations with dry states, Advances in Water Resources, 34 (2011) 1026-1038.

[110] D. Xiao, F. Fang, C. C. Pain, I. M. Navon, P. Salinas, A. Muggeridge, Non-intrusive reduced order modeling of multi-phase flow in porous media using the POD-RBF method, Submitted to J. Comput. Phys. (2015) .

[111] D. Xiao, F. Fang, A. G. Buchan, C. C. Pain, I. M. Navon, J. Du, G. H. Datum, Non-linear model reduction for the Navier-Stokes equations using residual DEIM method, J. Comput. Phys., 263 (2014) 1-18.

[112] D. Xiao, F. Fang, J. Du, C. C. Pain, I. M. Navon, A. G. Buchan, A. H. ElSheikh, G. H. Datum, Non-linear Petrov-Galerkin methods for reduced order modelling of the Navier-Stokes equations using a mixed finite element pair, Comput. Methods Appl. Mech. Engrg., 255 (2013) 147-157.

[113] D. Xiao, F. Fang, C. C. Pain, G. H. Datum, Non-intrusive reduced-order modelling of the Navier-Stokes equations based on RBF interpolation, International Journal for Numerical Methods in Fluids, 79 (2015) 580-595.

[114] D. Xiao, F. Fang, A. G. Buchan, C. C. Pain, I. M. Navon, A. Muggeridge, Non-intrusive reduced order modelling of the Navier-Stokes equations, Comput. Methods Appl. Mech. Engrg. 293 (2015) 522-541.

[115] Z. Wang, I. Akhtar, J. Borggaard, T. Iliescu, Proper orthogonal decomposition closure models for turbulent flows: a numerical comparison, Comput. Methods Appl. Mech. Engin., 237 (2012) 10-26.

[116] Z. Wang, Reduced-Order Modeling of Complex Engineering and Geophysical Flows: Analysis and Computations. PhD Thesis, Dept of Mathematics, 2012.

[117] Y. Wang, I. M. Navon, X. Wang, Y. Cheng, 2D Burgers equations with large Reynolds number using POD/DEIM and calibration, Int. J. Numer. Meth. Fluids, 2016, DOI: 10.1002/d.4249.

[118] Z. Wei, R. A Dalrymple, SPH modeling of short-crested waves, arXiv preprint arXiv:1705.08547, 2017.

[119] Z. Wei, R. A. Dalrymple, A. Herault, G. Bilotta, E. Rustico, H. Yeh, SPH modeling of dynamic impact of tsunami bore on bridge piers, Coastal Engineering 104 (2015) 26-42.

[120] Z. Wei, R. A. Dalrymple, Numerical study on mitigating tsunami force on bridges by an SPH model, Journal of Ocean Engineering and Marine Energy, 2 (2016) 365-380.

[121] Z. Wei, R. A. Dalrymple, E. Rustico, A. Herault, G. Bilotta, Simulation of near-shore tsunami breaking by smoothed particle hydrodynamics method, Journal of Waterway, Port, Coastal and Ocean Engineering, 142 (2016) Article number 05016001.

[122] Z. Wei, R. A. Dalrymple, SPH modeling of vorticity generation by short-crested wave breaking, Coastal Engineering Proceedings, 1 (2017).

[123] W. X. Wu, C. W. Shu, C. M. Wang, Vibration analysis of arbitrarily shaped membranes using local radial basis function–based differential quadrature method, Journal of Sound and Vibration, 306 (2007) 252–270.

[124] D. L. Young, S. P. Hu, C. S.Wu, Localized radial basis function scheme for multidimensional transient generalized newtonian fluid dynamics and heat transfer, Engin. Anal. Bound. Elem., 64 (2016) 68-89.

[125] Q. C. Zeng, Silt sedimentation and relevant engineering problem-an example of natural cybernetics, in: Proceedings of the Third International Congress on Industrial and Applied Mathematics, ICIAM95, Hamburg, Akademie Verlag, 1995, pp. 463–487.

[126] X. Zhang, H. Xiang, A fast meshless method based on proper orthogonal decomposition for the transient heat conduction problems, Int. J. Heat Mass Transfer, 84 (2015) 729-739.

[127] B. Zheng, B. D. Dai, A meshless local moving Kriging method for two-dimensional solids, Appl. Math. Comput., 218 (2011) 563-573.

[128] L. W. Zhang, K. M. Liew, An element-free based solution for nonlinear Schrodinger equations using the ICVMLS-Ritz method, Appl. Math. Comput., 249 (2014) 333-345.

[129] L. W. Zhang, Z. X. Lei, K. M. Liew, An element-free IMLS-Ritz framework for buckling analysis of FG-CNT reinforced composite thick plates resting on Winkler foundations, Eng. Anal. Bound. Elem., 58 (2015) 7-17.

[130] B. Zheng, B. Dai, A meshless local moving Kriging method for two-dimensional solids, Appl. Math. Comput., 218 (2011) 563-573.